Incident Response Planning Using a Lightweight Large Language Model with Reduced Hallucination

Kim Hammar†, Tansu Alpcan†, and Emil C. Lupu‡
† Department of Electrical and Electronic Engineering, University of Melbourne, Australia
‡ Department of Computing, Imperial College London, United Kingdom
Email: {kim.hammar,tansu.alpcan}@unimelb.edu.au and e.c.lupu@imperial.ac.uk

***Abstract*—Timely and effective incident response is key to managing the growing frequency of cyberattacks. However, identifying the right response actions for complex systems is a major technical challenge. A promising approach to mitigate this challenge is to use the security knowledge embedded in large language models (LLMs) to assist security operators during incident handling. Recent research has demonstrated the potential of this approach, but current methods are mainly based on prompt engineering of frontier LLMs, which is costly and prone to hallucinations. We address these limitations by presenting a novel way to use an LLM for incident response planning with reduced hallucination. Our method includes three steps: fine-tuning, information retrieval, and lookahead planning. We prove that our method generates response plans with a bounded probability of hallucination and that this probability can be made arbitrarily small at the expense of increased planning time under certain assumptions. Moreover, we show that our method is lightweight and can run on commodity hardware. We evaluate our method on logs from incidents reported in the literature. The experimental results show that our method a) achieves up to 22% shorter recovery times than frontier LLMs and b) generalizes to a broad range of incident types and response actions.**

I. Introduction

Incident response refers to the coordinated actions taken to contain, mitigate, and recover from cyberattacks. Today, incident response is largely a manual process carried out by security operators [1]. While this approach can be effective, it is often slow, labor-intensive, and requires significant skills. For example, a recent study reports that organizations take an average of 73 days to respond and recover from an incident [2]. Reducing this delay requires better decision-support tools to assist operators during incident handling. Currently, the standard approach to assisting operators relies on *response playbooks* [3], which comprise predefined rules for handling specific incidents. However, playbooks still rely on security experts for configuration and are therefore difficult to keep aligned with evolving threats and system architectures [4].

Network and Distributed System Security (NDSS) Symposium 2026
23-27 February 2026, San Diego, CA, USA
ISBN 979-8-9919276-8-0
https://dx.doi.org/10.14722/ndss.2026.240358
www.ndss-symposium.org

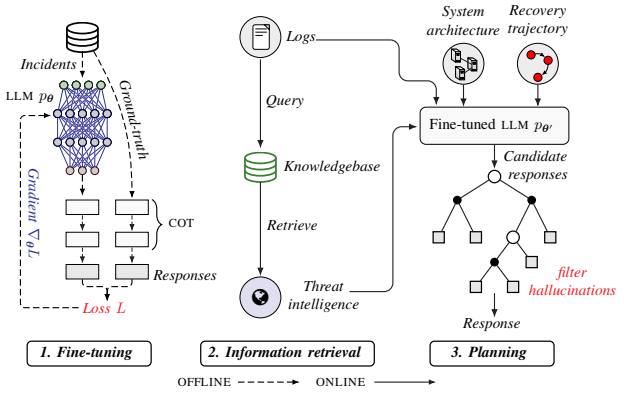

Fig. 1: The three steps of our method for incident response planning: 1. fine-tuning of a (lightweight) large language model (LLM); 2. retrieval of relevant threat intelligence; and 3. decision-theoretic planning and chain-of-thought (COT [5]) reasoning to select effective responses and filter hallucinations.

To overcome these limitations, an emerging direction of research is to leverage the security knowledge encoded in large language models (LLMs) to generate effective response actions [6]–[13]. These actions can then be used as suggestions to security operators. Although this approach remains largely confined to academic settings for now, it is beginning to see commercial adoption, as exemplified by IBM's recent launch of an LLM-based response service [14]. Most of the LLM-based methods proposed in the literature so far are based on prompt engineering of frontier LLMs, such as OPENAI O3 [15]. While this approach has shown promise, it is costly and relies on an external LLM provider (e.g., GOOGLE or OPENAI), which limits flexibility. Another important concern with this approach is that frontier LLMs are not specialized for incident response, which makes them particularly prone to *hallucinations* [16], i.e., they may generate response actions that appear plausible but are incorrect or unrelated to the incident.

In this paper, we present a novel method that addresses these limitations and provides a principled way to use an LLM as decision support for incident response; see Fig. 1. Our method includes three main steps: (*i*) instruction fine-tuning of a lightweight LLM to align it with the phases and objectives of incident response; (*ii*) retrieval-augmented generation (RAG) to ground the LLM in current threat information and system

knowledge; and (*iii*) decision-theoretic planning and chain-of-thought (COT) reasoning to generate effective response actions.

We evaluate our method based on log data from incidents reported in the literature. The results show that our method surpasses the performance of frontier LLMs (e.g., GEMINI 2.5 PRO [17], [18]) by up to 22% while being far less resource-intensive. Moreover, we show that our method performs comparably to the PPO reinforcement learning method [19], despite not relying on incident-specific training like PPO does. We also present an ablation study assessing the contribution of the individual steps of our method. We show that all steps contribute to its performance, with fine-tuning and planning having the greatest impact. In addition to the empirical results, we present a theoretical analysis that establishes a probabilistic upper bound on the hallucination probability of our method.

Our contributions can be summarized as follows:

- We develop a novel method for incident response that integrates a lightweight LLM with instruction fine-tuning, information retrieval, and decision-theoretic planning.
- We derive a probabilistic upper bound on the hallucination probability of our method. Under certain assumptions, this bound can be made arbitrarily small at the expense of increased planning time.
- We evaluate our method on logs from incidents reported in the literature. The results show that our method a) achieves up to 22% shorter recovery times than frontier LLMs; b) generalizes to a broad range of incidents and responses; and c) performs comparably to a reinforcement learning method that is pretrained for each incident.
- We release the first LLM fine-tuned for incident response, together with a dataset of $68,000$ incidents and the corresponding responses. Detailed instructions for accessing the dataset and reproducing our results are provided in Appendix F. We also provide source code and a video demonstration of a decision-support system that implements our method; see the repository at [20].

II. Related Work

Since the early 2000s, there has been broad interest in developing systems that can assist security operators during incident response [21], [22]. Traditional decision-support systems are based on playbooks that map incident scenarios to sequences of response actions [21], [23], such as those provided by SPLUNK [24], CISA [25], and OASIS [26]. Although playbooks can be effective, they rely on security experts for configuration. As a consequence, they are difficult to keep up-to-date with evolving security threats and system architectures [4]. Another common critique of playbooks is that they consist of generic response actions that are difficult for non-experts to interpret and execute effectively [3]. Several research efforts have aimed to address these limitations by *automating* the generation of effective incident response strategies and functions. Four predominant approaches to such automation have emerged: decision-theoretic [27], reinforcement learning [28], game-theoretic [29]–[31], and LLM-based approaches [6].

The first three approaches share a common requirement: they need a perfect simulator (model) that captures how the system evolves in response to attacks and defensive actions. The simulator enables the computation of optimal response strategies (according to the model) through numerical optimization techniques. For example, a standard benchmark in this line of research is CAGE-2 [32], which simulates an advanced persistent threat on an enterprise network. State-of-the-art methods evaluated on this benchmark include dynamic programming [33], reinforcement learning [34], and tree search [35], all of which rely on a simulator. While these approaches can be effective when high-fidelity simulators are available, such simulators are rarely available in practice. Furthermore, the resulting response strategies are limited in scope as they are trained on a narrow set of attack vectors and response options. For instance, the CAGE-2 simulation is limited to around 20 attacker actions and defensive countermeasures [35].

A promising approach to address this drawback is to use large language models (LLMs) to automatically generate effective response actions based on system logs. This approach is not limited to a predefined set of actions and eliminates the need for a simulator. Early studies in this direction include [6]–[12], and [14]. Notably, the work in [14] is a commercial product by IBM. While these works report encouraging results, they have three key limitations: they do not provide a theoretical analysis, they do not address the risk of hallucinations, and most of them require API access to frontier LLMs.

Our method differs from prior work in several ways. It does not rely on a simulator or a manually-designed playbook, is lightweight enough to run on commodity hardware, has reduced hallucination, is accompanied by a theoretical analysis, and combines fine-tuning with retrieval-augmented generation (RAG); see Table 1. Moreover, ours is the only LLM-based method that is fully open-source (code, weights, and data).

Method	*Theory*	RAG	*Fine-tuning*	*Lightweight*	LLM	*Req. simulator*	*Manual*
OURS (Fig. 1)	✓	✓	✓	✓	✓	✗	✗
[6],[7]–[11]	✗	✗	✗	✗	✓	✗	✗
[14]	✗	?	?	?	✓	✗	✗
[12]	✗	✓	✗	✗	✓	✗	✗
[33], [35], [36]	✓	✗	✗	✓	✗	✓	✗
[34],[28], [37]–[39]	✗	✗	✗	✓	✗	✓	✗
[23], [40], [41]	✗	✗	✗	✓	✗	✗	✓

TABLE 1: Comparison between our method and related approaches, which can be grouped into three categories: those relying on playbooks (white row), those relying on a simulator for numerical optimization (red rows), and those using LLMs (blue rows). Compared to other LLM-based approaches, our method (green row) is the only method that does not depend on frontier LLMs, is lightweight enough to run on commodity hardware, has reduced hallucination probability, and is accompanied by a theoretical analysis.

Lastly, we note that a growing body of research applies LLMs to security use cases other than incident response, such as penetration testing [42], [43], security assistants [44], scanning [45], [46], threat hunting [47], verification [48], piracy [49], detection [50], fuzzing [51], [52], API design [53], network operations [54], threat intelligence [55], and decompilation [56]. Compared to these works, the main novelty of our method lies in its approach to reducing hallucinations.

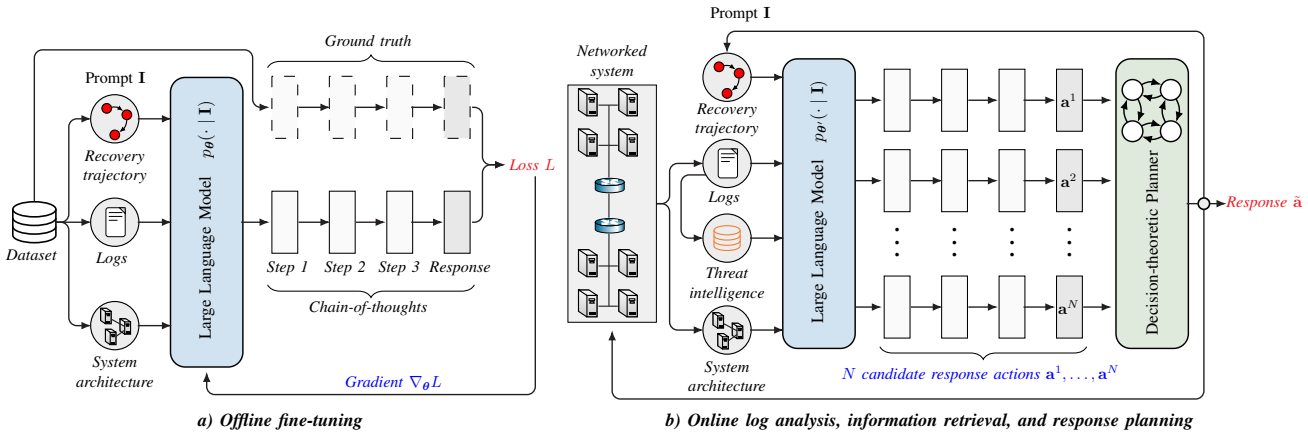

a) Offline fine-tuning *b) Online log analysis, information retrieval, and response planning*

Fig. 2: The two phases of our method. In the first phase [cf. **a**)], an LLM is fine-tuned offline on a dataset of logs from 68,000 incidents paired with response plans and chain-of-thought reasoning steps [5]. In the second phase [cf. **b**)], system logs and threat intelligence are processed online by the fine-tuned LLM and used to generate N candidate responses. These responses are then evaluated via a planning procedure, which selects the most effective response.

III. The Incident Response Problem

Incident response involves selecting a sequence of actions that restores a networked system to a secure and operational state after a cyberattack. These actions should analyze the scope of the attack, secure forensic evidence, contain and evict the attacker, harden the system to prevent recurrence, and restore critical services. Examples of response actions include redirecting network flows, updating access control policies, patching vulnerabilities, shutting down compromised systems, and restarting operational services. From a security engineering perspective [57], incident response fits within the broader cyber resilience framework by operationalizing the response and recovery phase after a cyberattack [58].

Figure 3 illustrates the phases of incident response. Following the attack are detection and response time intervals, which represent the time to detect the attack and form a response, respectively. These phases are followed by a *recovery time* interval T, during which response actions are deployed. When selecting these actions, the goal is to restore the system to a secure and operational state as quickly as possible while minimizing operational costs. A key challenge to achieving this goal is that the information about the attack is often limited to partial indicators of compromise (e.g., log files and alerts), while the full scope and severity of the attack are unknown [59]. Another major difficulty is that even short delays in initiating the response can lead to high costs. For example, in the event of a ransomware attack, a delay of just a few minutes may allow the malware to encrypt systems or spread laterally across the network [60].

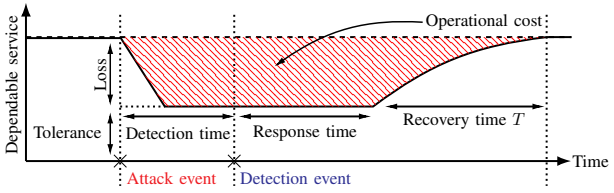

Fig. 3: Phases and performance metrics of the incident response problem.

IV. Our Method for Incident Response Planning

Motivated by the challenges described above, we develop a method for using an LLM as decision support during incident handling, i.e., to help security operators identify and execute effective response actions quickly. Broadly speaking, our method takes as input a description of an incident (e.g., system logs, security alerts, and threat intelligence) and produces as output a sequence of recommended response actions. The main challenge in generating such recommendations is to ensure that the response actions are effective despite the possibility that the LLM hallucinates. In the following subsections, we describe the steps we take to address this challenge.

A. Overview of Our Approach and System Architecture

Our method consists of three main steps: (*i*) supervised fine-tuning of a lightweight LLM to align it with the objectives of incident response; (*ii*) retrieval-augmented generation (RAG) to ground the LLM in current threat information and system knowledge; and (*iii*) decision-theoretic planning to synthesize effective response actions. These steps can be divided into two phases: an offline phase for fine-tuning and an online phase for information retrieval and response generation; see Fig. 2.

The first step of our method is to fine-tune a lightweight LLM for incident response. We conduct this fine-tuning by training the LLM on a labeled dataset of incident logs paired with corresponding response actions and reasoning steps. This training enables the LLM to learn typical patterns of incident handling. For example, it learns the logical dependencies between different phases of the response process, such as containment and eviction. Another benefit of fine-tuning is that it can reduce hallucinations; see e.g., [61].

Remark 1. *We call an* LLM lightweight *if it has significantly fewer parameters than a typical frontier* LLM. *For the experimental results reported in this paper, we use the* DEEPSEEK-R1-14B LLM, *which has* 14 *billion parameters. This parameter count is small in comparison with that of the frontier* LLM DEEPSEEK-R1, *which has* 671 *billion parameters [62].*

Once fine-tuned, the LLM can provide decision support for incident response by generating a sequence of recommended response actions when prompted with details about an incident. However, because the LLM is trained on historical incident data, it cannot generate response actions that relate to newly discovered vulnerabilities or attack techniques. To address this limitation, we augment the system logs with additional threat information retrieved online. Specifically, we automatically extract *indicators of compromise* from the logs (e.g., hostnames and vulnerability identifiers) and use them to retrieve relevant information from external sources, such as threat intelligence APIs and vulnerability databases. We then append this information to the logs before prompting the LLM. In addition to improving the quality of the response, several empirical studies have shown that such *retrieval-augmented generation* also reduces the probability of hallucinations [63].

Lastly, instead of directly selecting the response action generated by the fine-tuned LLM, we use the LLM to generate several candidate actions and select the most promising action that is least likely to be hallucinated. In particular, we evaluate each candidate action by using the LLM to simulate possible outcomes of the action, after which we select the action that leads to the shortest expected recovery time according to the lookahead simulations. This lookahead planning enforces a form of *self-consistency* [64], where actions are validated against the LLM's predicted outcomes. Such validation has been shown in prior work to reduce hallucinations; see e.g., [65], [66], and [67]. We provide a theoretical justification for why this procedure can reduce hallucination in §V.

Each of these three steps (fine-tuning, information retrieval, and planning) is detailed below, starting with fine-tuning.

B. Instruction Fine-Tuning

Our goal with fine-tuning is to make the pre-trained LLM generate appropriate response actions when prompted with system logs describing an incident. In this context, we view the pre-trained LLM as a probabilistic model that takes as input a sequence of tokens $\mathbf{x} = \mathbf{x}_1, \mathbf{x}_2, \ldots, \mathbf{x}_n$ and predicts the probability distribution over the subsequent token as

$$p_{\boldsymbol{\theta}}(\mathbf{x}_{n+1} \mid \mathbf{x}_1, \mathbf{x}_2, \ldots, \mathbf{x}_n), \tag{1}$$

where $\boldsymbol{\theta}$ denotes the model parameters.

The next-token prediction in (1) allows us to generate response actions as follows. We start by concatenating a description of the incident (e.g., system logs) with an instruction to generate a response action. We then pass the resulting text through a tokenizer that converts it into a sequence of tokens $\mathbf{x} = \mathbf{x}_1, \ldots, \mathbf{x}_n$. Next, we feed these tokens into the LLM to generate the next token by sampling from (1). Subsequently, we append the generated token to the prompt and feed the entire sequence back into the LLM to predict the next token. We repeat this process autoregressively until the LLM generates a special end-of-sequence token, which is produced when the LLM determines that the response action is complete, i.e., when the action has been fully specified.

Remark 2. *We place no restrictions on the form of a response action. It may be a single command, a compound procedure, or any other textual description, depending on the incident.*

To steer the LLM toward generating effective responses, we fine-tune it using supervised learning on a dataset of $68,000$ instruction-answer pairs $\mathcal{D} = \{(\mathbf{x}^i, \mathbf{y}^i)\}_{i=1}^{K}$, where each instruction $\mathbf{x}^i$ consists of information related to an incident and a task for the LLM to perform. The associated answer $\mathbf{y}^i$ describes the correct steps to complete the task, paired with a sequence of chain-of-thought (COT [5]) reasoning steps that explain the answer. We use two types of instructions: *action-generation* instructions and *state-prediction* instructions. In the former case, the vector $\mathbf{x}^i$ represents an instruction to generate a response to an incident. In the latter case, $\mathbf{x}^i$ represents an instruction to assess the current status of the incident response process. For example, the instruction may be to determine whether the attack has been contained, whether the system has been hardened to prevent recurrence, or whether forensic evidence has been secured.

Dataset generation.

To generate the training dataset for fine-tuning, we use a combination of log data from our testbed and synthetic data generated by frontier LLMs. Specifically, we first run a sequence of emulated cyberattacks (e.g., network intrusions) in our testbed, which generate system measurements and logs (e.g., SNORT alerts [68]). We then use these measurements to construct 500 instruction-answer pairs, e.g., pairs of incidents (described by log data) and suitable response actions.

Since these 500 pairs are too few for effective fine-tuning, we then expand the dataset using synthetic data generated by prompting GEMINI 2.5 PRO [17] and OPENAI O3 [15] with our initial examples. Following this approach, we construct a total dataset of $68,000$ incidents, which covers a diverse range of attack types and system architectures. Figure 4 shows the distributions of MITRE ATT&CK tactics [69] in our dataset, which shows that the most common attacker tactics are INITIAL ACCESS, EXECUTION, and EXFILTRATION.

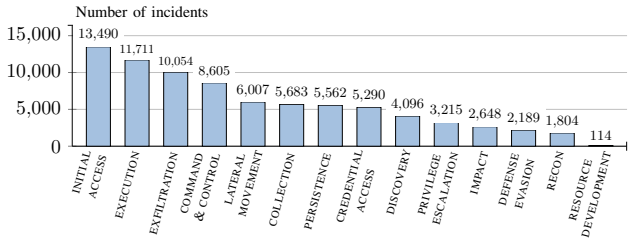

Fig. 4: Distributions of MITRE ATT&CK TACTICS [69] in our dataset of instruction-answer pairs $(\mathbf{x}, \mathbf{y})$, which we use for fine-tuning the LLM.

Our approach of combining log data with synthetic data is inspired by the studies presented in [70] and [71], which successfully used similar approaches to generate fine-tuning datasets for other domains, e.g., healthcare [71].

Testbed setup. To collect the initial log data for the fine-tuning, we run the attacks listed in Table 2 in a virtualized IT

Type	*Actions*	MITRE ATT&CK technique
Reconnaissance	TCP SYN scan, UDP scan	T1046 service scanning
	TCP XMAS scan	T1046 service scanning
	VULSCAN	T1595 active scanning
	ping-scan	T1018 system discovery
Brute-force	TELNET, SSH, FTP, IRC	T1110 brute force
	MONGODB, CASSANDRA	T1110 brute force
	SMTP, MYSQL, POSTGRES	T1110 brute force
Exploit	CVE-2017-7494, CVE-2015-3306	T1210 service exploitation
	CVE-2010-0426, CVE-2015-5602	T1068 privilege escalation
	CVE-2015-1427, CVE-2014-6271	T1210 service exploitation
	CVE-2016-10033, SQL injection	T1210 service exploitation

TABLE 2: Attacker actions executed on our testbed to generate the initial examples for our training dataset, which we use for fine-tuning the LLM. Actions are mapped to the corresponding vulnerabilities they exploit, as indicated by the CVE [72] identifiers and MITRE ATT&CK techniques [69].

infrastructure with 64 hosts that we deploy in our testbed; see Appendix A for the infrastructure configuration. Components of the infrastructure are implemented as DOCKER containers, which are connected in a network through virtual links. The attacks in Table 2 are automated through Python scripts that execute commands for accessing vulnerable services running in the containers. During each attack, we record SNORT alerts and other metrics by reading log files in the containers.

Fine-tuning results. Given the training dataset $\mathcal{D}$, we fine-tune the LLM by iteratively sampling a batch of instruction-answer pairs $(\mathbf{x}^1, \mathbf{y}^1), \ldots, (\mathbf{x}^M, \mathbf{y}^M)$ and updating its parameters via gradient descent based on the cross-entropy loss

$$L = -\frac{1}{M} \sum_{i=1}^{M} \sum_{k=1}^{m_i} \ln p_{\boldsymbol{\theta}} \left(\mathbf{y}_k^i \mid \mathbf{x}^i, \mathbf{y}_1^i, \ldots, \mathbf{y}_{k-1}^i \right), \qquad (2)$$

where m_i is the length of the vector $\mathbf{y}^i$. We denote the fine-tuned parameter vector by $\boldsymbol{\theta}'$ to distinguish it from $\boldsymbol{\theta}$.

Figure 5 displays the training loss curves when fine-tuning the DEEPSEEK-R1-14B LLM [62]. We run the experiment on 4×RTX 8000 GPUs and compare a higher learning rate (blue) with a lower one (red). We observe that the higher learning rate results in convergence to a lower loss. Additional experimental details and hyperparameters can be found in Appendix E.

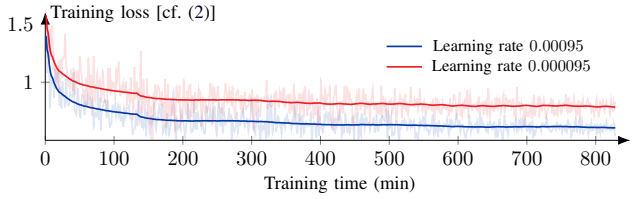

Fig. 5: Loss curves when fine-tuning the DEEPSEEK-R1-14B [62] LLM under two different learning rates. The solid lines indicate the mean loss and the shaded lines represent the loss on specific batches of training examples; cf. (2).

Figure 6 shows the accuracy and the F_1 score evaluated on a held-out set of 500 incidents from the training dataset. The accuracy is computed by comparing each generated response action with the correct action in the validation dataset. Similarly, the F_1 score is computed by checking if the generated

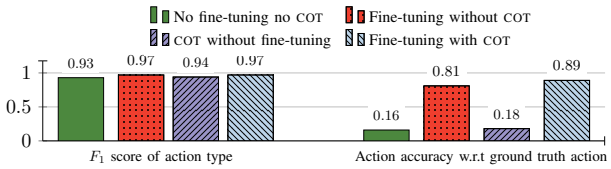

Fig. 6: The F_1 and accuracy scores on the validation dataset.

action is of the same type(s) as the correct action, which can be one or more of six types: containment, assessment, preservation, eviction, hardening, and restoration. We see in the figure that fine-tuning significantly improves the accuracy (from 0.16 to 0.89), whereas the improvement in the F_1 score is small in comparison (it increases from 0.93 to 0.97).

This result indicates that even before fine-tuning, the LLM is able to identify the correct type(s) of actions at each stage of the response with high probability. Hence, the primary benefit of fine-tuning in our setting is that it makes the LLM substantially better at adhering to the style of response actions in the training dataset, as quantified by the accuracy in Fig. 6.

Moreover, we observe in the figure that chain-of-thought (COT) reasoning has no substantial effect on the F_1 score but improves the accuracy from 0.81 to 0.89, which is a small improvement compared to that of fine-tuning. We explain this small improvement by the fact that COT does not update the LLM's weights as fine-tuning does. Similar results of fine-tuning and COT have been observed in prior work [71].

C. Retrieval-Augmented Response Generation (RAG)

While the fine-tuned LLM can generate effective response actions, its outputs depend on the distribution of incidents seen during training. This presents a limitation as the LLM is trained on historical data that may not reflect the most recent threat landscape. To address this challenge, we use indicators of compromise (e.g., vulnerability identifiers or hostnames) in the system logs to retrieve relevant threat intelligence from external sources. By incorporating such information at the time of action generation, the LLM can adapt its responses to reflect up-to-date threat information and system knowledge [73]. The RAG pipeline in our method is illustrated in Fig. 7.

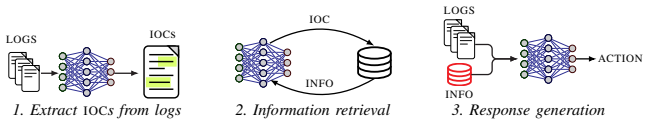

Fig. 7: Our RAG pipeline. The LLM extracts indicators of compromise from logs, retrieves related threat-intelligence data via APIs, appends it to the logs, and uses the enriched context to generate response actions.

To illustrate the benefit of RAG, consider a scenario where the LLM is trained on data available only up to 2020. Suppose that the LLM is prompted with information about an incident that relates to a vulnerability discovered after 2020, e.g., CVE-2021-44228 [72]. In this case, the LLM may not have sufficient information to generate effective response actions.

The following example contrasts the process of using the LLM to generate response actions with and without RAG:

- WITHOUT RAG. Prompted only with the logs, the LLM generates the action: "*isolate host*" as it has no knowledge about the nature of the vulnerability CVE-2021-44228.
- WITH RAG. The system retrieves information about specific mitigations for CVE-2021-44228. When provided with this information, the LLM generates a response action with targeted mitigations for CVE-2021-44228, thereby reducing the time to recover from the incident.

D. Incident Response Planning

Having fine-tuned the LLM to produce response actions from incident logs, we now address the challenge of selecting the most effective action. Although the LLM can produce effective actions in many cases, it may also hallucinate and generate ineffective actions. To reduce the risk of such hallucinations, our method includes a planning procedure where we use the LLM to generate multiple candidate actions and then select the action least likely to be hallucinated, as described below.

System model. We formulate incident response planning as a stochastic shortest path problem. In this formulation, the response process evolves over a sequence of *time steps* $t = 0, 1, \ldots, \tau$ and the goal is to generate a sequence of *actions* $\mathbf{a}_0, \mathbf{a}_1, \ldots, \mathbf{a}_{\tau-1}$ that quickly recovers the system from the incident. In other words, the goal is to minimize the *recovery time*. To formalize this goal, we model the progress toward system recovery with a *recovery state*. We define this state based on the MITRE D3FEND [74] taxonomy as follows.

Definition 1 (Recovery state)**.** *The recovery state is a vector*

$$\mathbf{s}_t = (s_t^{\mathrm{I}}, s_t^{\mathrm{S}}, s_t^{\mathrm{F}}, s_t^{\mathrm{E}}, s_t^{\mathrm{H}}, s_t^{\mathrm{R}}), \tag{3}$$

where each component is a value in $[0, 1]$ *representing the progress toward completing a specific stage of the response. A value of* 0 *indicates no progress, while* 1 *indicates that the stage is completed. The stages are defined as follows.*

- ***Containment****:* $s_t^{\mathrm{I}} \in [0, 1]$ *is the degree to which the attack has been isolated and prevented from spreading.*
- ***Assessment****:* $s_t^{\mathrm{S}} \in [0, 1]$ *is the degree to which the scope and severity of the attack have been determined.*
- ***Preservation****:* $s_t^{\mathrm{F}} \in [0, 1]$ *is the degree to which forensic evidence related to the incident has been preserved.*
- ***Eviction****:* $s_t^{\mathrm{E}} \in [0, 1]$ *is the degree to which the attacker's access has been revoked and potential malicious code or processes have been removed from the system.*
- ***Hardening****:* $s_t^{\mathrm{H}} \in [0, 1]$ *is the degree to which the system has been hardened to prevent recurrence of the attack.*
- ***Restoration****:* $s_t^{\mathrm{R}} \in [0, 1]$ *is the degree to which services have been restarted and user access has been restored.*

Remark 3. *While the analysis presented in this paper focuses on the state representation in Def. 1, our method is not limited to this choice and can accommodate alternative ways of representing the state, such as dependency graphs.*

Given the preceding definition of the recovery state, we associate each response action $\mathbf{a}_t$ with a cost $c(\mathbf{s}_t, \mathbf{a}_t)$, which represents the time required to execute it in state $\mathbf{s}_t$. This cost function allows our model to assign different time units to individual actions. For instance, the time to isolate a compromised host may be a few seconds, whereas the time to perform a forensic analysis of affected systems can be several hours. In practice, the cost function c can be configured using time estimates based on previous incidents or exercises.

The *recovery time* T is the cumulative time required to complete all stages of the response, i.e., the time to reach the *terminal state* $\mathbf{s} = (1, 1, 1, 1, 1, 1)$, as formally defined below.

Definition 2 (Recovery time)**.** *The recovery time* T *represents the time to reach the terminal recovery state, i.e.,*

$$T = \sum_{t=0}^{\tau-1} c(\mathbf{s}_t, \mathbf{a}_t), \tag{4}$$

where τ *is the number of actions to recover, i.e.,*

$$\tau = \inf\{t \mid t > 0, \mathbf{s}_t = (1, 1, 1, 1, 1, 1)\}.$$

We illustrate this definition through the following example.

Example 1 (Recovery time)**.** *Consider a response plan with four actions:* $\mathbf{a}_0$ *(assessment and containment),* $\mathbf{a}_1$ *(preservation),* $\mathbf{a}_2$ *(eviction and hardening), and* $\mathbf{a}_3$ *(restoration). Suppose that the incident response team has determined based on previous incidents and red-teaming exercises that*

- ***Assessment and containment****, which mainly involve automated shell commands, typically take about a minute;*
- ***Preservation****, which requires forensic disk imaging and copying large amounts of data, takes about 2 hours;*
- ***Eviction and hardening****, which involve system scans and configuration updates, take around 25 minutes; and*
- ***Restoration****, which involves restarting services and validating user access, usually completes within 5 minutes.*

Using these estimates, our method can be instantiated with the action costs $c(\mathbf{s}_0, \mathbf{a}_0) = 1$ *min,* $c(\mathbf{s}_1, \mathbf{a}_1) = 120$ *min,* $c(\mathbf{s}_2, \mathbf{a}_2) = 25$ *min, and* $c(\mathbf{s}_3, \mathbf{a}_3) = 5$ *min. In this case, the estimated recovery time* T *is calculated through* (4) *as*

$$T = \sum_{t=0}^{3} c(\mathbf{s}_t, \mathbf{a}_t) = 1 + 120 + 25 + 5 = 151 \text{ min}.$$

The recovery time provides a general metric to compare different incident response plans. While no single metric can capture all dimensions of incident response, the recovery time is widely used in both research and practice as an indicator of recovery performance; see e.g., [2], [14], [75]. Moreover, the recovery time can be complemented with additional performance metrics that reflect specific organizational goals, such as risk preferences or service availability constraints. Such metrics can be incorporated in our model by encoding them as cost functions and adding them to the sum in (4).

To illustrate our system model, we show two possible state trajectories $\mathbf{s}_0, \mathbf{s}_1, \ldots, \mathbf{s}_\tau$ in Fig. 8. As shown in the figure, several response actions may achieve the same effect on the recovery state. For example, the severity of the attack can be determined in many ways. Moreover, certain response actions can lead to shorter recovery times by skipping intermediate

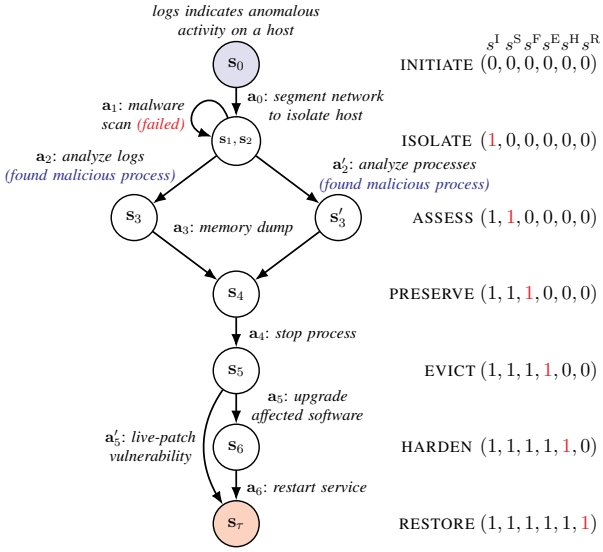

Fig. 8: Two example evolutions of the recovery state $\mathbf{s}_t$; cf. (3). The first recovery trajectory involves the actions $\mathbf{a}_0, \mathbf{a}_1, \mathbf{a}_2, \mathbf{a}_3, \mathbf{a}_4, \mathbf{a}_5, \mathbf{a}_6$ and the second trajectory involves the actions $\mathbf{a}_0, \mathbf{a}_1, \mathbf{a}'_2, \mathbf{a}_3, \mathbf{a}_4, \mathbf{a}'_5$.

steps. For instance, in the event of a denial of service (DOS) attack, containment and eviction can often be achieved simultaneously by appropriate filtering of the network traffic. This single action both isolates the attack ($s_t^{\mathrm{I}} = 1$) and revokes attacker access ($s_t^{\mathrm{E}} = 1$). In contrast, an advanced persistent threat (APT) typically requires multiple actions to complete these stages. For example, containment may involve isolating compromised hosts ($s_t^{\mathrm{I}} = 1$) and eviction may require malware removal or credential rotation ($s_t^{\mathrm{E}} = 1$). Thus, the recovery time T for an APT is typically longer than for a DOS attack.

While the examples in Fig. 8 illustrate actions that fully complete certain response stages, in practice, actions may also lead to partial completions of different stages. For example, an initial containment attempt such as blocking suspicious network traffic may only partially isolate the attack ($s_t^{\mathrm{I}} < 1$). Likewise, an assessment action, such as scanning system logs, may only partially determine the scope of the attack ($s_t^{\mathrm{S}} < 1$). Hence, Def. 1 and Def. 2 capture the interdependence of response stages and the incremental progress across them.

Moreover, since a response action can include multiple steps, our model can also capture the parallelization of response stages. Such parallelization can reduce the total recovery time by avoiding sequential execution of response stages, as illustrated in the following two examples.

Example 2 (Parallelization of containment and assessment)**.** *Consider a response action* $\mathbf{a}$ *that includes steps for both isolating hosts (a containment step that takes* 2 *hours) and analyzing logs (an assessment step that takes* 3 *hours). Given such a compound action, we can model the parallelization of the containment and assessment stages of incident response by setting the time cost* $c(\mathbf{s}, \mathbf{a})$ *to the duration of the longest step in the action* $\mathbf{a}$ *(3 hours) rather than the combined duration (5 hours), which reduces the time to complete the containment and assessment stages in our model from* 5 *hours to* 3 *hours.*

In general, the reduction in recovery time achieved by parallelizing response stages depends on the specific incident, the systems involved, and the stages that are parallelized.

We illustrate a real-world case of response parallelization using the WANNACRY incident that affected UK's health service in 2017, as it is one of the few publicly documented incidents that provides a detailed timeline of the response.

Example 3 (Parallelization of containment, hardening, and restoration)**.** *In the response to the* WANNACRY *incident that affected* UK*'s national health service in 2017, the containment, hardening, and restoration stages were carried out in parallel by different actors [60, Fig. 2]. According to the post-incident report, fully restoring services took roughly a week, while containment took about* 8 *hours and hardening (patching) took about* 5 *days. Because these response stages proceeded concurrently rather than sequentially, the overall recovery time was reduced from about two weeks to one week.*

Response generation. Because the recovery state contains information about the attacker, it is generally not known with certainty. However, the LLM can predict the state based on the available system logs and threat intelligence, which we denote by $\mathbf{I}$. Such predictions allow us to generate a response plan through auto-regressive sampling as follows. We start by generating the first action as $\mathbf{a}_0 \sim p_{\boldsymbol{\theta}'}(\cdot \mid \mathbf{s}_0, \mathbf{I})$, where the initial state is $\mathbf{s}_0 = (0,0,0,0,0,0)$. Subsequently, we evaluate the effect of the action by predicting the next recovery state as $\tilde{\mathbf{s}}_1 \sim p_{\boldsymbol{\theta}'}(\cdot \mid \mathbf{s}_0, \mathbf{a}_0, \mathbf{I})$. We then repeat the same procedure to generate the next action as $\mathbf{a}_1 \sim p_{\boldsymbol{\theta}'}(\cdot \mid \tilde{\mathbf{s}}_1, \mathbf{I})$. This iterative procedure continues until the LLM predicts that the terminal recovery state $\tilde{\mathbf{s}}_t = (1,1,1,1,1,1)$ has been reached.

The expected time to recover from the incident when using response actions generated by the LLM depends on the current recovery state $\mathbf{s}_t$ (which captures the effects of previous actions) and the type of incident, as characterized by the vector $\mathbf{I}$. We formally define this recovery time-to-go as follows.

Definition 3 (Recovery time-to-go)**.** *Given an incident described by* $\mathbf{I}$*, the expected recovery time-to-go from the state* $\mathbf{s}$ *when executing actions generated by the* LLM $p_{\boldsymbol{\theta}'}$ *is*

$$J(\mathbf{s}) = \begin{cases} 0 & \text{if } \mathbf{s} = (1,1,1,1,1,1), \\ \mathbb{E}_{\mathbf{a}_t \sim p_{\boldsymbol{\theta}'}(\cdot \mid \tilde{\mathbf{s}}_t, \mathbf{I})} \{T \mid \mathbf{s}_0 = \mathbf{s}, \mathbf{I}\} & \text{otherwise.} \end{cases}$$

Given this definition, we say that a response action is *hallucinated* if it has no effect on the expected recovery time-to-go. In other words, it does not contribute any progress toward recovery. This notion is formally defined below.

Definition 4 (Hallucinated response action)**.** *A response action* $\mathbf{a}_t$ *is hallucinated if it leads to a recovery state with the same expected recovery time-to-go as the current state, i.e.,*

$$J(\mathbf{s}_t) - \mathbb{E}_{\mathbf{s}_{t+1}} \{J(\mathbf{s}_{t+1}) \mid \mathbf{a}_t, \mathbf{s}_t, \mathbf{I}\} = 0, \quad \text{for all } \mathbf{s}_t \in \tilde{\mathcal{S}},$$

where $\tilde{\mathcal{S}}$ *denotes the set of all states except* $(1,1,1,1,1,1)$.

This definition implies that hallucinations can be avoided by generating actions until one is found that reduces the expected recovery time-to-go. However, this approach to reducing hallucinations is not feasible in practice, as computing the recovery time requires knowledge of the attacker's behavior.

To circumvent this limitation, we adopt a different approach, known as *self-verification* [66]. Following this approach, we *estimate* the recovery time-to-go of response actions using the LLM itself. This verification enforces a form of *self-consistency* [64], where actions are validated against the LLM's predicted outcomes. Such validations have been shown to reduce hallucinations (see e.g., [65] and [67]) and form the basis for our planning algorithm, as described below. (For a theoretical justification of why this approach can reduce the probability of hallucinated response actions, see §V.)

Planning algorithm. At each time t of the response, we use the LLM to generate N candidate actions $\mathcal{A}_t^N = \{\mathbf{a}_t^1, \ldots, \mathbf{a}_t^N\}$. Then, for each action $\mathbf{a}_t^i$, we use the LLM to simulate M *recovery trajectories* $\tilde{\mathbf{s}}_{t+1}, \mathbf{a}_{t+1} \ldots$, by sampling actions and updating the state until $\tilde{\mathbf{s}}_T = (1,1,1,1,1,1)$. We then use the average length of the simulated trajectories as an estimate of the expected recovery time-to-go. We define this estimate as

$$\tilde{Q}(\tilde{\mathbf{s}}_t, \mathbf{a}_t^i) \approx c(\tilde{\mathbf{s}}_t, \mathbf{a}_t^i) + \sum_{\mathbf{s}_{t+1} \in \mathcal{S}} p_{\boldsymbol{\theta}'}(\mathbf{s}_{t+1} \mid \tilde{\mathbf{s}}_t, \mathbf{a}_t^i, \mathbf{I}) \tilde{J}(\mathbf{s}_{t+1}),$$

where $\tilde{J}$ is the estimated time-to-go function and $\tilde{Q}(\mathbf{s}, \mathbf{a})$ is the estimated time-to-go when taking action $\mathbf{a}$ in state $\mathbf{s}$.

Finally, we select the action with the shortest expected recovery time-to-go according to the estimate, i.e.,

$$\tilde{\mathbf{a}}_t \in \arg\min_{\mathbf{a}_t^i \in \mathcal{A}_t^N} \tilde{Q}(\tilde{\mathbf{s}}_t, \mathbf{a}_t^i). \tag{5}$$

This planning procedure is illustrated conceptually in Fig. 9 and the pseudocode is listed in Alg. 1. In the next section, we analyze the theoretical properties of this procedure and establish conditions under which it reduces hallucination. We also derive a bound on its hallucination probability.

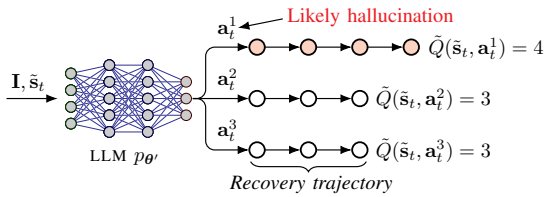

Fig. 9: Our planning procedure. At each response step, the LLM is prompted with the incident description $\mathbf{I}$ and the predicted recovery state $\tilde{\mathbf{s}}_t$ to generate N candidate actions (here $N = 3$). For each action $\mathbf{a}_t^i$, we estimate the expected recovery time-to-go $\tilde{Q}(\tilde{\mathbf{s}}_t, \mathbf{a}_t^i)$ by simulating recovery trajectories with the LLM. We then select the action that leads to the shortest trajectory.

V. Analysis of the Hallucination Probability

To analyze the probability that our method generates a hallucinated response action, we distinguish between two cases: (*i*) at least one of the N candidate actions is non-hallucinated; and (*ii*) all N actions are hallucinated; cf. (5). In the following, we establish a sufficient condition under which hallucinations are avoided in case (*i*), and derive a probabilistic upper bound on the probability that case (*ii*) occurs.

Algorithm 1: Incident response planning with an LLM.

Input: LLM $p_{\boldsymbol{\theta}'}$, system logs $\mathbf{I}$, # actions N, # samples M.
Output: A response plan ρ, i.e., a sequence of response actions.
Initialize $\tilde{\mathbf{s}}_0 \leftarrow (0,0,0,0,0,0), \rho \leftarrow \emptyset, t \leftarrow 0$.
while $\tilde{\mathbf{s}}_t \neq (1,1,1,1,1,1)$ **do**
  Sample $\mathbf{a}_t^1, \ldots, \mathbf{a}_t^N$ from $p_{\boldsymbol{\theta}'}(\cdot \mid \tilde{\mathbf{s}}_t, \mathbf{I})$.
  for $i = 1, 2, \ldots, N$ **do**
    $\tilde{Q}(\tilde{\mathbf{s}}_t, \mathbf{a}_t^i) = \frac{1}{M} \sum_{k=1}^{M}$ RECOVERY-TIME$(\tilde{\mathbf{s}}_t, \mathbf{a}_t^i, \mathbf{I})$.
  end
  Select action $\tilde{\mathbf{a}}_t \in \arg\min_{\mathbf{a}_t^i} \tilde{Q}(\tilde{\mathbf{s}}_t, \mathbf{a}_t^i)$, $\rho \leftarrow \rho \cup \{(t, \tilde{\mathbf{a}}_t)\}$.
  Update the state as $\tilde{\mathbf{s}}_{t+1} \sim p_{\boldsymbol{\theta}'}(\cdot \mid \tilde{\mathbf{s}}_t, \tilde{\mathbf{a}}_t, \mathbf{I})$, $t \leftarrow t+1$.
end
return ρ.
Procedure RECOVERY-TIME $(\tilde{\mathbf{s}}, \mathbf{a}, \mathbf{I})$
  Predict the state as $\tilde{\mathbf{s}}' \sim p_{\boldsymbol{\theta}'}(\cdot \mid \tilde{\mathbf{s}}, \mathbf{a}, \mathbf{I})$.
  if $\tilde{\mathbf{s}}' = (1,1,1,1,1,1)$ **then**
    return $c(\tilde{\mathbf{s}}', \mathbf{a})$.
  end
  else
    Sample $\mathbf{a}'$ from $p_{\boldsymbol{\theta}'}(\cdot \mid \tilde{\mathbf{s}}', \mathbf{I})$.
    return $c(\tilde{\mathbf{s}}', \mathbf{a}) +$ RECOVERY-TIME$(\tilde{\mathbf{s}}', \mathbf{a}', \mathbf{I})$.
  end
end

A. Sufficient Conditions for Filtering Hallucinations

The purpose of the minimization (5) is to filter *hallucinated actions*, i.e., actions that do not affect the recovery time. This filtering is effective when the lookahead simulations [cf. lines 13–22 in Alg. 1] accurately reflect that hallucinated actions have no beneficial impact on the expected recovery time. However, because these simulations rely on the LLM to predict action outcomes, the filtering is inherently imperfect. Consequently, the effectiveness of the planning step [cf. (5)] depends on two key factors: (*i*) the degree to which hallucinated and non-hallucinated actions can be distinguished based on their impact on expected recovery time; and (*ii*) the accuracy of the LLM's predictions of the resulting recovery state $\mathbf{s}_t$; cf. Def. 1.

To quantify these two factors, let $\mathcal{A}$ denote the set of all possible response actions (as defined by the vocabulary of the LLM) and let $\mathcal{A}(\mathbf{s}, \mathbf{I})$ be the subset of non-hallucinated actions for the incident described by $\mathbf{I}$, given the recovery state $\mathbf{s}$. Moreover, let δ denote the minimal change in the recovery time-to-go when taking a non-hallucinated action, i.e.,

$$\delta = \min \left\{ J(\mathbf{s}_t) - \mathbb{E}_{\mathbf{s}_{t+1}} \left\{ J(\mathbf{s}_{t+1}) \mid \mathbf{a}, \mathbf{s}_t, \mathbf{I} \right\} \,\middle|\, \mathbf{a} \in \mathcal{A}(\mathbf{s}, \mathbf{I}) \right\}.$$

In view of Def. 4, we have $\delta > 0$.

Similarly, let η denote the total variation between the LLM's predictions and the true system dynamics (denoted by P), i.e.,

$$\sum_{\mathbf{s}' \in \mathcal{S}} \left| p_{\boldsymbol{\theta}'}(\mathbf{s}' \mid \mathbf{s}, \mathbf{a}, \mathbf{I}) - P(\mathbf{s}' \mid \mathbf{s}, \mathbf{a}, \mathbf{I}) \right| \leq \eta, \quad \forall \mathbf{s} \in \tilde{\mathcal{S}}, \mathbf{a} \in \mathcal{A},$$

where $\mathcal{S}$ is the set of all recovery states and $\tilde{\mathcal{S}}$ is the set of non-terminal recovery states, i.e., $\tilde{\mathcal{S}} = \mathcal{S} \setminus \{(1,1,1,1,1,1)\}$. Note that the parameter η is upper bounded by 2, i.e., $0 \leq \eta \leq 2$.

Given the parameters δ and η, we have the following result.

Proposition 1. *Assuming that a) the number of sample trajectories M in Alg. 1 is sufficiently large so that the empirical mean approximates the true expectation and b) that both the expected recovery time and the* LLM*'s predicted recovery time are finite, i.e., $\|J\|_\infty < \infty$ and $\|\tilde{J}\|_\infty < \infty$. If at least one action in the set $\mathcal{A}_t^N$ [cf. (5)] is non-hallucinated and*

$$\delta > 2\eta \|J\|_\infty \left(\|\tilde{J}\|_\infty + 1 \right),$$

then the action selected by Alg. 1 will be non-hallucinated.

We present the proof of Prop. 1 in Appendix C. This proposition provides a sufficient condition under which the minimization (5) effectively filters hallucinated actions. The main condition of the proposition is that δ (which captures the degree to which hallucinations and non-hallucinations can be distinguished) is sufficiently large in comparison with the inaccuracy of the LLM's predictions, as quantified by η. While these parameters are likely unknown in practice, they can be estimated based on traces of historical incidents. We provide pseudocode for estimating δ and η in Alg. 2. The algorithm iterates over a labeled dataset of incidents and uses the LLM to predict recovery states and their recovery time-to-go. In particular, the estimate $\hat{\delta}$ is updated based on the difference between the predicted time-to-go of non-hallucinated actions and hallucinated ones (line 6). Similarly, the estimate $\hat{\eta}$ is computed as the maximum prediction error (line 7).

Algorithm 2: Estimation of parameters δ and η.

1 **Input:** LLM $p_{\boldsymbol{\theta}'}$, incident dataset $\mathcal{D}$. **Output:** Parameters $\hat{\delta}, \hat{\eta}$.
2 Initialize $\hat{\delta} \leftarrow \infty$, $\hat{\eta} \leftarrow 0$.
3 **foreach** *incident* $(\mathbf{I}, \mathbf{s}_0, \rho) \in \mathcal{D}$ **do**
4 **foreach** *step in the response plan* ρ **do**
5 Predict the state $\tilde{\mathbf{s}}'$ and time-to-go $\tilde{J}(\tilde{\mathbf{s}}')$ of actions.
6 $\hat{\delta} \leftarrow \min_{\mathbf{a}\,\text{(non-hallucinated)}} \{\hat{\delta}, \tilde{J}(\tilde{\mathbf{s}}_t) - \tilde{J}(\tilde{\mathbf{s}}')\}$.
7 $\hat{\eta} \leftarrow \max_{\mathbf{a}} \sum_{\mathbf{s}' \in \mathcal{S}} \left| p_{\boldsymbol{\theta}'}(\tilde{\mathbf{s}}' \mid \tilde{\mathbf{s}}_t, \mathbf{a}, \mathbf{I}) - P(\mathbf{s}' \mid \mathbf{s}_t, \mathbf{a}, \mathbf{I}) \right|$.
8 **end**
9 **end**
10 **return** $\hat{\delta}, \hat{\eta}$.

If at least one action in the set $\mathcal{A}_t^N$ [cf. (5)] would always be non-hallucinated, Prop. 1 would imply a condition that provides a guarantee of avoiding hallucinations. However, in practice, it is possible that all actions in $\mathcal{A}_t^N$ are hallucinated, in which case the lookahead minimization (5) will not help. We quantify the probability of this event in the next subsection.

B. Upper Bound on the Hallucination Probability

To complement the above condition for filtering hallucinations, we now analyze the *hallucination probability*. The main difficulty in this analysis is that the LLM's propensity to hallucinate is not known a priori. For this reason, we base our analysis on empirical observations of its behavior.

To obtain such empirical observations, we start by using the LLM to generate L sample actions. We then verify how many of those actions are hallucinated to estimate the LLM's hallucination probability h. We denote this estimate by $\overline{h}$. Due to sampling variability, this estimate may differ substantially from the probability h. To address this possibility, we establish a bound that quantifies how likely it is for the estimate $\overline{h}$ to deviate from the hallucination probability h by more than a given threshold ϵ, as stated in the following proposition.

Proposition 2. *Let h denote the true (but unknown) hallucination probability of the* LLM *and let $\overline{h}$ denote the empirical probability based on L samples. We have*

$$P(h \geq \overline{h} + \epsilon) \leq e^{-2\epsilon^2 L},$$

where $\epsilon > 0$ is a configurable parameter.

Proof. We model the process of generating L actions and verifying which of them are hallucinated as L independent and identically distributed Bernoulli trials, represented by the random variables $X_1, X_2, \ldots, X_L$. We have $X_i = 1$ if the ith sampled action is hallucinated; $X_i = 0$ otherwise. Hence, $\overline{h} = \frac{1}{L} \sum_{i=1}^{L} X_i$. Applying Hoeffding's inequality, we have

$$P(h \geq \overline{h} + \epsilon) \leq e^{-2\epsilon^2 L}.$$

□

This proposition implies that the probability that all actions in the set $\mathcal{A}_t^N$ [cf. (5)] are hallucinated (i.e., h^N) can be controlled with a certain confidence when the conditions of Prop. 1 hold by increasing N. Moreover, the confidence increases exponentially with the number of samples L used to estimate the hallucination probability, as shown in Fig. 10.

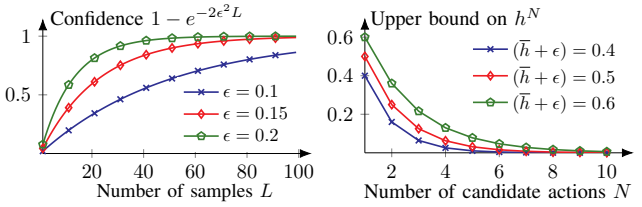

Fig. 10: Illustration of Prop. 2. Here L is the number of samples for estimating the hallucination probability and N is the number of candidate actions; cf. (5).

VI. Summary of Our Method

In summary, our method for using an LLM as decision support during incident handling consists of three main steps:

1) *Offline instruction fine-tuning of a lightweight* LLM.
   - We fine-tune the LLM via supervised learning on a dataset of logs from $68,000$ incidents paired with response plans and chain-of-thought reasoning steps.
2) *Online information retrieval.*
   - Before prompting the LLM with system logs to generate candidate response actions, we enrich the logs with threat intelligence retrieved from external sources.
3) *Online lookahead planning via Alg. 1.*
   - Instead of directly executing the action generated by the fine-tuned LLM, we generate several candidate actions and select the one that leads to the shortest predicted recovery time, which reduces the probability of hallucinations under certain conditions; cf. Prop. 1.

Dataset	*System*	*Attacks*	*Logs*
CTU-Malware-2014 [76]	WINDOWS XP SP2 servers	Various malwares and ransomwares, e.g., CRYPTODEFENSE [77].	SNORT alerts [68]
CIC-IDS-2017 [78]	WINDOWS and LINUX servers	Denial-of-service, web attacks, heartbleed, SQL injection, etc.	SNORT alerts [68]
AIT-IDS-V2-2022 [79]	LINUX and WINDOWS servers/hosts	Multi-stage attack with reconnaissance, cracking, and escalation.	WAZUH alerts [80]
CSLE-IDS-2024 [81]	LINUX servers	SAMBACRY, SHELLSHOCK, exploit of CVE-2015-1427, etc.	SNORT alerts [68]

TABLE 3: The datasets of cyberattacks and logs used for the experimental evaluation.

Method	*Number of parameters*	*Context window size*
OUR METHOD	14 billion	128,000
DEEPSEEK-R1 [62]	671 billion [62]	128,000
GEMINI 2.5 PRO [17]	unknown ($\geq$ 100 billion)	1 million
OPENAI O3 [15]	unknown ($\geq$ 100 billion)	200,000

TABLE 4: Comparison between our method and frontier LLMs.

VII. Experimental Evaluation of Our Method

In this section, we present an experimental evaluation of our method. We start by comparing its performance with that of frontier LLMs based on log data from incidents reported in the literature. We then compare the performance of our method with that of a popular reinforcement learning method on the CAGE-2 benchmark [32], namely proximal policy optimization (PPO) [19]. Our main evaluation metric is the recovery time T, as defined in Def. 2. We measure the recovery time in discrete time units, assigning a time of 1 to all actions except those that include superfluous steps, which we assign a time of 2. This time structure allows us to evaluate the decision-making efficiency of our method without making assumptions about system-specific execution times, which vary between different implementations and are not the focus of this paper.

We instantiate our method with the DEEPSEEK-R1-14B LLM [62], which we fine-tune using the procedure described in §IV-B. Further, we implement the RAG pipeline described in §IV-C using the open threat exchange (OTX) API [82]. Finally, we instantiate the planning procedure described in Alg. 1 with $N = 3$ candidate actions and $M = 3$ samples; cf. (5). Additional experimental details and hyperparameters are provided in Appendix E and Appendix F.

A. Comparison with Frontier LLMs

We compare our method with three frontier LLMs: DEEPSEEK-R1 [62], GEMINI 2.5 PRO [17], and OPENAI O3 [15]. Compared to these models, the main difference is that our method is significantly more lightweight; see Table 4.

Evaluation datasets. The evaluation is based on log data from 25 incidents across 4 different datasets published in the literature, namely CTU-Malware-2014 [76], CIC-IDS-2017 [78], AIT-IDS-V2-2022 [79], and CSLE-IDS-2024 [81]; see Table 3 and Fig. 11. We also include 5 false-positive incidents. Each incident contains log data and a brief system description. Given this data, the task of the LLM is to generate effective response actions, which we compare against the ground truth.

The logs in these datasets are generated during controlled executions of real cyberattacks, such as software exploits, network intrusions, denial-of-service attacks, and ransomware attacks; see Table 3. They are established benchmarks in the research community, which ensures that our results are reproducible and can be compared with alternative methods. For example, the CIC-IDS-2017 dataset is cited by more than 5,500 papers and is available as a benchmark problem on Kaggle with over 90 submissions [78]. While evaluation in a security operations center (SOC) would provide additional insights, it involves sensitive data and does not allow reproducible experiments or comparison with alternative methods. Therefore, we focus on the benchmark datasets in this paper and leave the evaluation in a SOC for future work. For an empirical study on the usage of LLMs in incident response based on interviews with SOC analysts, we refer to [13].

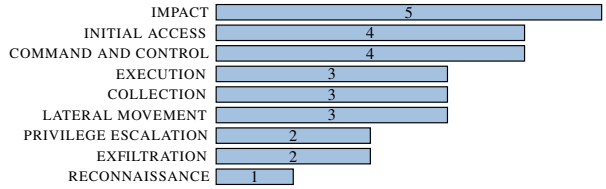

Fig. 11: Occurrences of MITRE ATT&CK TACTICS in the evaluation datasets.

We provide a (condensed) example of an incident from the CTU-Malware-2014 dataset [76] on the next page. In this example, the (ground truth) response plan consists of 6 response actions. Hence, the shortest possible recovery time an LLM can achieve when evaluated on this example is $T = 6$. However, if the LLM generates a plan that includes unnecessary response actions, then the recovery time will be longer than 6. It is also possible that the generated actions fail to fully recover the system from the incident. We report such cases separately in the evaluation results.

Evaluation results. The results are summarized in Fig. 12. Across all evaluation datasets, our method achieves the shortest average recovery time. On average, the recovery time of our method is 13.46 compared to 16.21 for the next best method. Among the frontier LLMs, we observe that GEMINI 2.5 PRO performs best on average, whereas the difference between OPENAI O3 and DEEPSEEK-R1 is not statistically significant.

Scalability analysis. Figure 13 shows the compute time per time step of Alg. 1 for varying number of candidate actions N. We observe that the planning time increases linearly with N when the actions are evaluated sequentially. However, by parallelizing the computation across multiple GPUs, the planning time remains nearly constant as N increases.

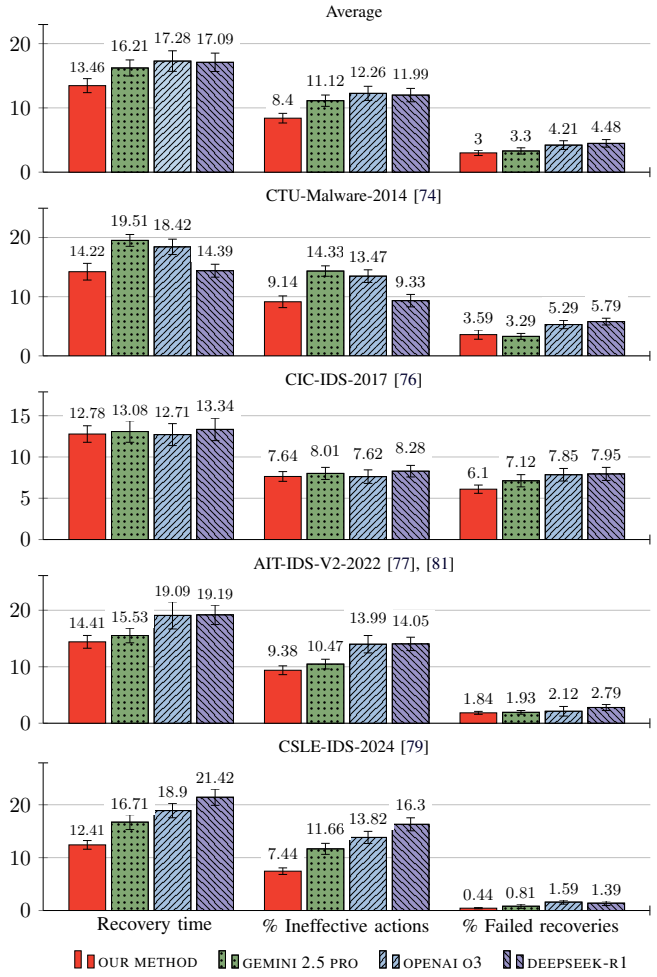

Fig. 12: Evaluation results (↓ better): comparison between our method and frontier LLMs. Bar colors relate to different methods; bar groups indicate performance metrics; numbers and error bars indicate the mean and the standard deviation from 5 evaluations with different random seeds.

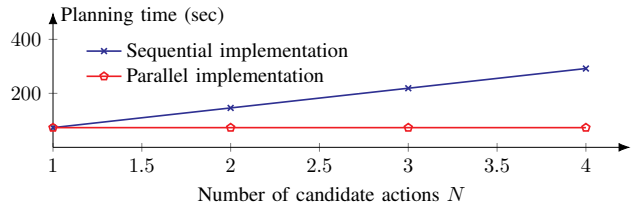

Fig. 13: Time required (per time step) to execute Alg. 1 for varying number of candidate actions N. The average planning times were computed based on 5 executions with RTX 8000 GPUs.

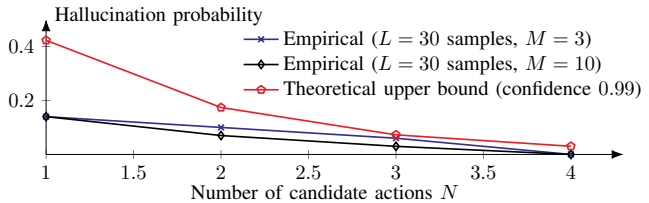

Fig. 14: The empirical hallucination probability of our method for varying number of candidate actions N, as well as the theoretical upper bound on the hallucination probability h^N (assuming the conditions of Prop. 1 hold) with confidence 0.99, i.e., the right-hand side of the bound in Prop. 2 is 0.01.

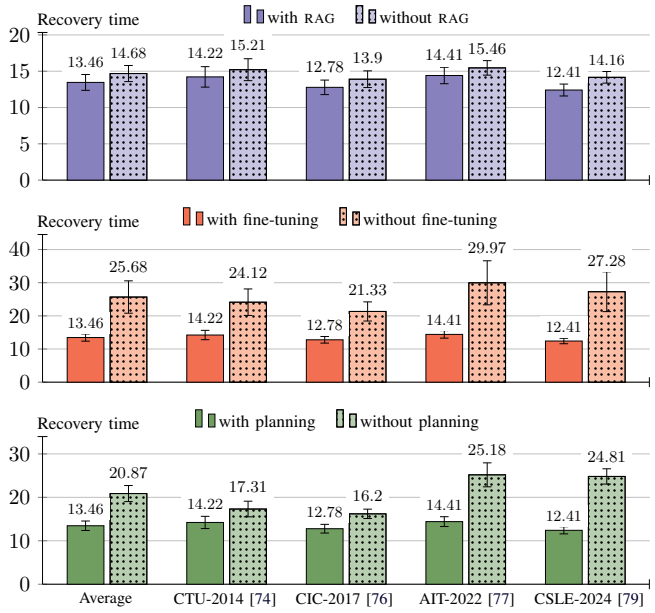

Fig. 15: Ablation-study results for the recovery time metric (↓ better). Bars relate to our method with and without different steps; bar groups indicate the evaluation dataset; numbers and error bars indicate the mean and the standard deviation from 5 evaluations with different random seeds.

Example incident from the CTU-Malware-2014 dataset [76].

System description (condensed): Two subnetworks (A and B) are connected via a switch that is also connected to the Internet. All servers run WINDOWS XP SP2. Their IPs and configurations are...

Snort alert logs (condensed):

```
[120:3:2] (http_inspect) NO CONTENT-LENGTH..
[1:31033:6] MALWARE Win.Trojan.Cryptodefence..
{TCP} 147.32.84.165:1057 -> 222.88.205.195:443
[129:5:1] Bad segment, adjusted size..
[139:1:1] (spp_sdf) SDF..
```

Incident summary: Server 147.32.84.165 is infected with the WIN.TROJAN.CRYPTODEFENCE ransomware. Alerts show the server is making outbound command and control (C2) connections to 222.88.205.195. This indicates that the ransomware is active and may be preparing to encrypt files or has already begun doing so.

Response actions (condensed):

1. Disconnect the Ethernet cable of the infected server at 147.32.84.165 to sever its network connection. Concurrently, configure a rule on the main switch/firewall to block all outbound traffic to the C2 server 222.88.205.195.

2. Analyze the central switch to scan all network traffic from both subnetworks A and B for any other hosts attempting to make connections to the malicious IP 222.88.205.195.

3. Before altering the infected server, create a complete bit-for-bit forensic image of its hard drive. This preserves the ransomware executable, encrypted files, and other evidence for future analysis.

4. Wipe the hard drive of 147.32.84.165. If other infected machines were discovered, they must also be taken offline and wiped.

5. Upgrade all servers from WINDOWS XP SP2 (which is obsolete) to a modern operating system that receives security patches.

6. Restore the server's data from a trusted backup. Once the server is rebuilt with a modern operating system, reconnect it to the network and closely monitor for any anomalous activity.

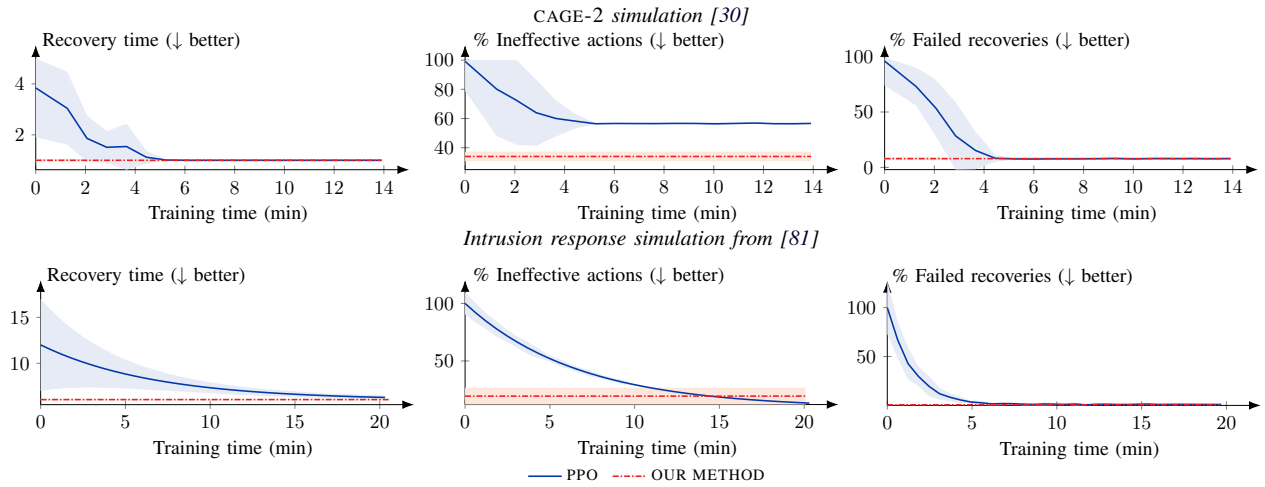

Fig. 16: Comparison between our method (red curves) and the PPO reinforcement learning method (blue curves) [19]. The first row of plots relates to the CAGE-2 simulation [32] and the second row relates to the network intrusion simulation from [83]. Columns relate to different evaluation metrics (↓ better). Curves show the mean value from evaluations with 5 random seeds; shaded areas indicate standard deviations. The x-axes indicate the training time required by PPO for each simulation. In contrast, our method requires no incident-specific training.

Hallucination analysis. Figure 14 shows the empirical hallucination probability of our method based on $L = 30$ response actions sampled from the LLM when prompted with log data from the evaluation datasets. The figure also shows the theoretical upper bound expressed in Prop. 2.

We observe in Fig. 14 that the theoretical bound holds uniformly over the empirical probabilities. However, the bound is not tight, as expected. We used $M = 3$ and $M = 10$ samples to estimate the expected recovery times in Alg. 1. As shown in the figure, increasing M reduces the hallucination probability.

Ablation study. To evaluate the importance of each step of our method (i.e., fine-tuning, RAG, and planning), we evaluate our method with and without each step. The results are summarized in Fig. 15. We observe performance degradations when each step is removed. The most substantial degradation occurs when fine-tuning is removed, which causes the average recovery time to increase from 13 to 25. Planning also has a significant impact. Without planning, the average recovery time jumps from 13 to 21. Retrieval-augmented generation (RAG) contributes as well, though its effects are more modest.

B. Comparison with Proximal Policy Optimization

Numerous reinforcement learning approaches have been proposed for incident response, including policy optimization methods [34], tree search [35], stochastic approximation [83], and Q-learning [37]; see [84] for an extensive review of the state of the art. Among these methods, variants of proximal policy optimization (PPO) [19] dominate recent work. We therefore use PPO as a representative baseline for comparison.

Experiment setup. We evaluate our method against PPO on two simulated incidents: an advanced persistent threat from the CAGE-2 simulation [32], and a network intrusion scenario from [83]. The evaluation uses the same metrics as in the comparison with frontier LLMs[1]. The hyperparameters of PPO that we use for the evaluation are available in Appendix E.

Evaluation results. The results are presented in Fig. 16. Both our method and PPO achieve similar performance in terms of recovery time and failed recoveries across the two simulations. The only notable performance gap is in the percentage of ineffective actions for the CAGE-2 simulation, where our method performs better. The key difference between our method and PPO lies in their training requirements: PPO requires incident-specific training (approximately 10–20 minutes of training per incident) to reach good performance. In contrast, our method does not require such training to achieve good performance.

C. Discussion of the Evaluation Results

Our experimental results demonstrate a trade-off between generality, computational cost, and deployment practicality. Compared to frontier LLMs, our method is significantly more lightweight, i.e., it requires fewer parameters and runs efficiently on commodity hardware, yet it achieves consistently better performance across all evaluation metrics. This performance advantage is primarily driven by our fine-tuning and planning steps, as shown in the ablation study; cf. Fig. 15.

When compared to reinforcement learning methods such as PPO, our method is more computationally costly at inference time due to the overhead of planning; see Fig. 13. However, this overhead is offset by a major advantage: our method requires no incident-specific training. In contrast, PPO must be retrained for each new incident, which is impractical.

Takeaways. In summary, our main experimental findings are:

- Our method consistently outperforms frontier LLMs across all evaluation metrics, while being significantly more lightweight and able to run on commodity hardware.

[1]To align the CAGE-2 scenario with our evaluation metrics, we exclude decoy-related actions as they target prevention rather than response.

- Fine-tuning and decision-theoretic planning are key drivers of performance, RAG is less important.
- Compared to reinforcement learning methods, our method has higher overhead but avoids incident-specific training.

D. Comparison with Incident Response Playbooks

From an operational point of view, our method can be seen as a more dynamic and actionable complement to incident response playbooks [23], which makes it easy to adopt in existing SOC workflows [13]. In the following, we describe the main similarities and advantages of our method in comparison with conventional incident response playbooks.

Similarities. Both the response plans generated by our method and playbooks are expressed in text and organized around the standard stages of incident response, such as containment, assessment, and eviction. Moreover, both our method and playbooks are intended to provide decision support rather than automating the response. Another similarity is that both of them categorize attacks according to the MITRE ATT&CK taxonomy. Despite these similarities, our method provides several advantages over playbooks, as listed below.

Advantages. The main advantage is that our method does not rely on domain experts for configuration, as playbooks do. This makes our method more flexible. Another benefit is that our method generates more precise and context-specific response actions than playbooks, which often prescribe vague actions that are not directly executable, as reported in several empirical studies; see e.g., [3], [4]. By contrast, our method produces executable actions tailored to the system logs, which helps the operator to prioritize log entries. As a consequence, our method provides a higher degree of automation than conventional playbooks, shifting the operator's role toward validating the generated response plan rather than sifting through logs. Beyond these advantages, a fundamental difference between our method and playbooks is that a response plan generated by our method typically spans 2–3 pages, whereas playbooks often span 40+ pages (see e.g., [25]), many of which contain information that is not directly relevant to the response (e.g., general security principles). Thus, our method serves as a more actionable complement to conventional playbooks.

Limitations. A concern with LLM-based systems is the risk of hallucination, which limits their reliability in fully autonomous operation. Our method mitigates this issue through fine-tuning, information retrieval, and planning, which substantially reduces the probability of hallucination and improves reliability. However, fully autonomous incident response remains challenging due to the inherent complexity of many incidents, which makes human oversight necessary for critical decisions.

VIII. Conclusion

We introduce a novel method that enables the effective use of a large language model (LLM) to provide decision support for incident response planning. Our method uses the LLM for translating system logs into effective response plans while addressing its limitations through fine-tuning, information retrieval, and decision-theoretic planning. We prove that our method produces incident responses with bounded hallucination probability; see Prop. 1 and Prop. 2. Under certain assumptions, this bound can be made arbitrarily small at the expense of increased planning time. We evaluate our method on logs from incidents reported in the literature. The results show that our method a) achieves up to 22% shorter recovery times than frontier LLMs and b) generalizes to a broad range of incident types and response actions.

Future work. A primary direction for future work is to conduct evaluations in operational settings, where security operators use our method for decision support. Such studies would provide insights into the practical utility of our method and how to improve it further. From a theoretical standpoint, a promising direction of future work is to tighten the hallucination-probability bound stated in Prop. 2. A possible approach to tighten this bound is to leverage conformal-abstention techniques [85]. Another direction for future work is to extend the system model in §IV-D to include additional performance metrics beyond recovery time. Moreover, due to the generality of our method, it is possible to extend our planning procedure [cf. Alg. 1] in many ways, e.g., by incorporating rollout techniques [86] or tree search [35]. Similarly, the information-retrieval step of our method can be expanded to integrate information from several sources.

Acknowledgment

This research is supported by the Swedish Research Council under contract 2024-06436.

References

[1] D. W. Woods, R. Böhme, J. Wolff, and D. Schwarcz, "Lessons lost: Incident response in the age of cyber insurance and breach attorneys," in *32nd USENIX Security Symposium (USENIX Security 23)*. Anaheim, CA: USENIX Association, Aug. 2023, pp. 2259–2273. [Online]. Available: https://www.usenix.org/conference/usenixsecurity23/presentation/woods

[2] IBM Security and P. Institute, "Cost of a data breach report 2024," IBM, Cambridge, MA, Tech. Rep. 19, 2024, based on breaches at 524 organizations between March 2023 and February 2024.

[3] R. Stevens, D. Votipka, J. Dykstra, F. Tomlinson, E. Quartararo, C. Ahern, and M. L. Mazurek, "How ready is your ready? assessing the usability of incident response playbook frameworks," in *Proceedings of the 2022 CHI Conference on Human Factors in Computing Systems*, ser. CHI '22. New York, NY, USA: Association for Computing Machinery, 2022. [Online]. Available: https://doi.org/10.1145/3491102.3517559

[4] D. Schlette, P. Empl, M. Caselli, T. Schreck, and G. Pernul, "Do you play it by the books? a study on incident response playbooks and influencing factors," in *2024 IEEE Symposium on Security and Privacy (SP)*, 2024, pp. 3625–3643.

[5] J. Wei, X. Wang, D. Schuurmans, M. Bosma, B. Ichter, F. Xia, E. H. Chi, Q. V. Le, and D. Zhou, "Chain-of-thought prompting elicits reasoning in large language models," in *Proceedings of the 36th International Conference on Neural Information Processing Systems*, ser. NIPS '22. Red Hook, NY, USA: Curran Associates Inc., 2022.

[6] S. R. Castro, R. Campbell, N. Lau, O. Villalobos, J. Duan, and A. A. Cardenas, "Large language models are autonomous cyber defenders," 2025. [Online]. Available: https://arxiv.org/abs/2505.04843

[7] M. Rigaki, O. Lukáš, C. A. Catania, and S. Garcia, "Out of the cage: How stochastic parrots win in cyber security environments," 2023, https://arxiv.org/abs/2308.12086.

[8] H. Mohammadi, J. J. Davis, and M. Kiely, "Leveraging large language models for autonomous cyber defense: Insights from CAGE-2 simulations," *IEEE Intelligent Systems*, pp. 1–8, 2025.

[9] Y. Yan, Y. Zhang, and K. Huang, "Depending on yourself when you should: Mentoring LLM with RL agents to become the master in cybersecurity games," 2024. [Online]. Available: https://arxiv.org/abs/2403.17674

[10] S. Hays and J. White, "Employing LLMs for incident response planning and review," 2024. [Online]. Available: https://arxiv.org/abs/2403.01271

[11] X. Lin, J. Zhang, G. Deng, T. Liu, X. Liu, C. Yang, T. Zhang, Q. Guo, and R. Chen, "IRCopilot: Automated incident response with large language models," 2025. [Online]. Available: https://arxiv.org/abs/2505.20945

[12] J. F. Loevenich, E. Adler, R. Mercier, A. Velazquez, and R. R. F. Lopes, "Design of an autonomous cyber defence agent using hybrid AI models," in *2024 International Conference on Military Communication and Information Systems (ICMCIS)*, 2024, pp. 1–10.

[13] D. Kramer, L. Rosique, A. Narotam, E. Bursztein, P. G. Kelley, K. Thomas, and A. Woodruff, "Integrating large language models into security incident response," in *Proceedings of the Twenty-First USENIX Conference on Usable Privacy and Security*, ser. SOUPS '25. USA: USENIX Association, 2025.

[14] S. Hussey. (2025, June) Resolve incidents faster with IBM Instana intelligent incident investigation powered by agentic AI. [Online]. Available: https://www.ibm.com/new/announcements/resolve-incidents-faster-with-ibm-instana-intelligent-incident-investigation-powered-by-agentic-ai

[15] OpenAI, J. Achiam, S. Adler *et al.*, "GPT-4 technical report," 2024. [Online]. Available: https://arxiv.org/abs/2303.08774

[16] G. Sriramanan, S. Bharti, V. S. Sadasivan, S. Saha, P. Kattakinda, and S. Feizi, "LLM-check: Investigating detection of hallucinations in large language models," in *Advances in Neural Information Processing Systems*, A. Globerson, L. Mackey, D. Belgrave, A. Fan, U. Paquet, J. Tomczak, and C. Zhang, Eds., vol. 37, 2024, pp. 34 188–34 216. [Online]. Available: https://proceedings.neurips.cc/paper_files/paper/2024/file/3c1e1fdf305195cd620c118aaa9717ad-Paper-Conference.pdf

[17] G. Comanici, E. Bieber *et al.*, "Gemini 2.5: Pushing the frontier with advanced reasoning, multimodality, long context, and next generation agentic capabilities," 2025. [Online]. Available: https://arxiv.org/abs/2507.06261

[18] G. Team, R. Anil, S. Borgeaud *et al.*, "Gemini: A family of highly capable multimodal models," 2024, https://arxiv.org/abs/2312.11805. [Online]. Available: https://arxiv.org/abs/2312.11805

[19] J. Schulman, F. Wolski, P. Dhariwal, A. Radford, and O. Klimov, "Proximal policy optimization algorithms," *CoRR*, 2017. [Online]. Available: http://arxiv.org/abs/1707.06347

[20] K. Hammar, T. Alpcan, and E. C. Lupu, "Supplementary material of the paper "Incident Response Planning Using a Lightweight Large Language Model with Reduced Hallucination"," 2026, artifact repository: https://doi.org/10.5281/zenodo.17459636, Code: https://github.com/Kim-Hammar/llm_incident_response_ndss26, dataset: https://huggingface.co/datasets/kimhammar/CSLE-IncidentResponse-V1, video demonstration: https://www.youtube.com/watch?v=e7ckmv5p6cI, fine-tuned LLM and prompts: https://huggingface.co/kimhammar/LLMIncidentResponse.

[21] N. Stakhanova, S. Basu, and J. Wong, "A taxonomy of intrusion response systems," *Int. J. Inf. Comput. Secur.*, vol. 1, no. 1/2, p. 169–184, Jan. 2007. [Online]. Available: https://doi.org/10.1504/IJICS.2007.012248

[22] T. Alpcan and T. Basar, "A game theoretic approach to decision and analysis in network intrusion detection," in *42nd IEEE International Conference on Decision and Control (IEEE Cat. No.03CH37475)*, vol. 3, 2003, pp. 2595–2600 Vol.3.

[23] A. Applebaum, S. Johnson, M. Limiero, and M. Smith, "Playbook oriented cyber response," in *2018 National Cyber Summit (NCS)*, 2018, pp. 8–15.

[24] Splunk, "Automate incident response with playbooks and actions in splunk mission control," 2025, https://help.splunk.com/en/splunk-enterprise-security-7/mission-control/investigate-and-respond-to-threats/automate-incident-response/automate-incident-response-with-playbooks-and-actions-in-splunk-mission-control.

[25] CISA, "Cybersecurity incident & vulnerability response playbooks," 2021, https://www.cisa.gov/resources-tools/resources/federal-government-cybersecurity-incident-and-vulnerability-response-playbooks.

[26] OASIS, "Cacao security playbooks version 2.0," 2023, https://docs.oasis-open.org/cacao/security-playbooks/v2.0/security-playbooks-v2.0.html.

[27] K. Hammar and R. Stadler, "Intrusion tolerance for networked systems through two-level feedback control," in *2024 54th Annual IEEE/IFIP International Conference on Dependable Systems and Networks (DSN)*, 2024, pp. 338–352.

[28] A. V. Singh, E. Rathbun, E. Graham, L. Oakley, S. Boboila, A. Oprea, and P. Chin, "Hierarchical multi-agent reinforcement learning for cyber network defense," 2024. [Online]. Available: https://arxiv.org/abs/2410.17351

[29] K. Hammar, T. Li, R. Stadler, and Q. Zhu, "Adaptive security response strategies through conjectural online learning," *IEEE Transactions on Information Forensics and Security*, vol. 20, pp. 4055–4070, 2025.

[30] S. A. Zonouz, H. Khurana, W. H. Sanders, and T. M. Yardley, "RRE: A game-theoretic intrusion response and recovery engine," in *2009 IEEE/IFIP International Conference on Dependable Systems & Networks*, 2009, pp. 439–448.

[31] T. Alpcan and T. Basar, *Network Security: A Decision and Game-Theoretic Approach*, 1st ed. USA: Cambridge University Press, 2010.

[32] CAGE, "TTCP CAGE challenge 2," in *AAAI-22 Workshop on Artificial Intelligence for Cyber Security (AICS)*, 2022, https://github.com/cage-challenge/cage-challenge-2.

[33] K. Hammar, Y. Li, T. Alpcan, E. C. Lupu, and D. Bertsekas, "Adaptive network security policies via belief aggregation and rollout," 2025. [Online]. Available: https://arxiv.org/abs/2507.15163

[34] S. Vyas, J. Hannay, A. Bolton, and P. P. Burnap, "Automated cyber defence: A review," 2023.

[35] K. Hammar, N. Dhir, and R. Stadler, "Optimal defender strategies for CAGE-2 using causal modeling and tree search," 2024. [Online]. Available: https://arxiv.org/abs/2407.11070

[36] T. Li, K. Hammar, R. Stadler, and Q. Zhu, "Conjectural online learning with first-order beliefs in asymmetric information stochastic games," in *2024 IEEE 63rd Conference on Decision and Control (CDC)*, 2024, pp. 6780–6785.

[37] A. Applebaum, C. Dennler, P. Dwyer, M. Moskowitz, H. Nguyen, N. Nichols, N. Park, P. Rachwalski, F. Rau, A. Webster, and M. Wolk, "Bridging automated to autonomous cyber defense: Foundational analysis of tabular Q-learning," in *Proceedings of the 15th ACM Workshop on Artificial Intelligence and Security*, 2022. [Online]. Available: https://doi.org/10.1145/3560830.3563732

[38] A. Ramamurthy and N. Dhir, "General autonomous cybersecurity defense: Learning robust policies for dynamic topologies and diverse attackers," 2025. [Online]. Available: https://arxiv.org/abs/2506.22706

[39] Z. Huang, J. Robin, N. Herbaut, N. B. Rabah, and B. L. Grand, "Toward an intent-based and ontology-driven autonomic security response in security orchestration automation and response," 2025. [Online]. Available: https://arxiv.org/abs/2507.12061

[40] A. Shaked, Y. Cherdantseva, and P. Burnap, "Model-based incident response playbooks," in *Proceedings of the 17th International Conference on Availability, Reliability and Security*, ser. ARES '22. New York, NY, USA: Association for Computing Machinery, 2022. [Online]. Available: https://doi.org/10.1145/3538969.3538976

[41] M. Akbari Gurabi, L. Nitz, A. Bregar, J. Popanda, C. Siemers, R. Matzutt, and A. Mandal, "Requirements for playbook-assisted cyber incident response, reporting and automation," *Digital Threats*, vol. 5, no. 3, Oct. 2024. [Online]. Available: https://doi.org/10.1145/3688810

[42] G. Deng, Y. Liu, V. Mayoral-Vilches, P. Liu, Y. Li, Y. Xu, T. Zhang, Y. Liu, M. Pinzger, and S. Rass, "PentestGPT: Evaluating and harnessing large language models for automated penetration testing," in *33rd USENIX Security Symposium (USENIX Security 24)*. Philadelphia, PA: USENIX Association, Aug. 2024, pp. 847–864. [Online]. Available: https://www.usenix.org/conference/usenixsecurity24/presentation/deng

[43] M. Rodriguez, R. A. Popa, F. Flynn, L. Liang, A. Dafoe, and A. Wang, "A framework for evaluating emerging cyberattack capabilities of AI," 2025. [Online]. Available: https://arxiv.org/abs/2503.11917

[44] J. Deng, X. Li, Y. Chen, Y. Bai, H. Weng, Y. Liu, T. Wei, and W. Xu, "RACONTEUR: A knowledgeable, insightful, and portable LLM-powered shell command explainer," in *32nd Annual Network and Distributed System Security Symposium, NDSS 2025, San Diego, California, USA, February 24-28, 2025*. The Internet Society, 2025. [Online]. Available: https://www.ndss-symposium.org/ndss-paper/raconteur-a-knowledgeable-insightful-and-portable-llm-powered-shell-command-explainer/

[45] A. Stafeev, T. Recktenwald, G. D. Stefano, S. Khodayari, and G. Pellegrino, "YuraScanner: Leveraging LLMs for task-driven web app scanning," in *32nd Annual Network and Distributed System Security Symposium, NDSS 2025, San Diego, California, USA, February 24-28, 2025*. The Internet Society, 2025. [Online]. Available: https://www.ndss-symposium.org/ndss-paper/yurascanner-leveraging-llms-for-task-driven-web-app-scanning/

[46] P. Liu, J. Liu, L. Fu, K. Lu, Y. Xia, X. Zhang, W. Chen, H. Weng, S. Ji, and W. Wang, "Exploring ChatGPT's capabilities on vulnerability management," in *33rd USENIX Security Symposium (USENIX Security 24)*. Philadelphia, PA: USENIX Association, Aug. 2024, pp. 811–828. [Online]. Available: https://www.usenix.org/conference/usenixsecurity24/presentation/liu-peiyu

[47] M. Allamanis, M. Arjovsky, C. Blundell *et al.*, "From naptime to big sleep: Using large language models to catch vulnerabilities in real-world code," 2024, https://googleprojectzero.blogspot.com/2024/10/from-naptime-to-big-sleep.html.

[48] Y. Liu, Y. Xue, D. Wu, Y. Sun, Y. Li, M. Shi, and Y. Liu, "PropertyGPT: LLM-driven formal verification of smart contracts through retrieval-augmented property generation," in *32nd Annual Network and Distributed System Security Symposium, NDSS 2025, San Diego, California, USA, February 24-28, 2025*. The Internet Society, 2025. [Online]. Available: https://www.ndss-symposium.org/ndss-paper/propertygpt-llm-driven-formal-verification-of-smart-contracts-through-retrieval-augmented-property-generation/

[49] V. Gohil, M. DeLorenzo, V. V. A. S. V. Nallam, J. See, and J. Rajendran, "LLMPirate: LLMs for black-box hardware IP piracy," in *32nd Annual Network and Distributed System Security Symposium, NDSS 2025, San Diego, California, USA, February 24-28, 2025*. The Internet Society, 2025. [Online]. Available: https://www.ndss-symposium.org/ndss-paper/llmpirate-llms-for-black-box-hardware-ip-piracy/

[50] Y. Yang, J. Liu, K. Chen, and M. Lin, "The midas touch: Triggering the capability of LLMs for RM-API misuse detection," in *32nd Annual Network and Distributed System Security Symposium, NDSS 2025, San Diego, California, USA, February 24-28, 2025*. The Internet Society, 2025. [Online]. Available: https://www.ndss-symposium.org/ndss-paper/the-midas-touch-triggering-the-capability-of-llms-for-rm-api-misuse-detection/

[51] C. S. Xia, M. Paltenghi, J. Le Tian, M. Pradel, and L. Zhang, "Fuzz4all: Universal fuzzing with large language models," in *Proceedings of the IEEE/ACM 46th International Conference on Software Engineering*, ser. ICSE '24. New York, NY, USA: Association for Computing Machinery, 2024. [Online]. Available: https://doi.org/10.1145/3597503.3639121

[52] X. Ma, L. Luo, and Q. Zeng, "From one thousand pages of specification to unveiling hidden bugs: Large language model assisted fuzzing of matter IoT devices," in *33rd USENIX Security Symposium (USENIX Security 24)*. Philadelphia, PA: USENIX Association, Aug. 2024, pp. 4783–4800. [Online]. Available: https://www.usenix.org/conference/usenixsecurity24/presentation/ma-xiaoyue

[53] J. Liu, Y. Yang, K. Chen, and M. Lin, "Generating API parameter security rules with LLM for API misuse detection," in *32nd Annual Network and Distributed System Security Symposium, NDSS 2025, San Diego, California, USA, February 24-28, 2025*. The Internet Society, 2025. [Online]. Available: https://www.ndss-symposium.org/ndss-paper/generating-api-parameter-security-rules-with-llm-for-api-misuse-detection/

[54] D. Wu, X. Wang, Y. Qiao, Z. Wang, J. Jiang, S. Cui, and F. Wang, "NetLLM: Adapting large language models for networking," in *Proceedings of the ACM SIGCOMM 2024 Conference*, ser. ACM SIGCOMM '24. New York, NY, USA: Association for Computing Machinery, 2024, p. 661–678. [Online]. Available: https://doi.org/10.1145/3651890.3672268

[55] M. Arazzi, D. R. Arikkat, S. Nicolazzo, A. Nocera, R. Rehiman K.A., V. P., and M. Conti, "NLP-based techniques for cyber threat intelligence," *Computer Science Review*, vol. 58, p. 100765, 2025. [Online]. Available: https://www.sciencedirect.com/science/article/pii/S1574013725000413

[56] P. Hu, R. Liang, and K. Chen, "DeGPT: Optimizing decompiler output with LLM," in *31st Annual Network and Distributed System Security Symposium, NDSS 2024, San Diego, California, USA, February 26 - March 1, 2024*. The Internet Society, 2024. [Online]. Available: https://www.ndss-symposium.org/ndss-paper/degpt-optimizing-decompiler-output-with-llm/

[57] R. J. Anderson, *Security Engineering: A Guide to Building Dependable Distributed Systems*, 1st ed. USA: John Wiley & Sons, Inc., 2001.

[58] A. A. Ganin, E. Massaro, A. Gutfraind, N. Steen, J. M. Keisler, A. Kott, R. Mangoubi, and I. Linkov, "Operational resilience: concepts, design and analysis," *Scientific Reports*, vol. 6, no. 1, p. 19540, Jan 2016. [Online]. Available: https://doi.org/10.1038/srep19540

[59] L. Li, X. Zhang, X. Zhao, H. Zhang, Y. Kang, P. Zhao, B. Qiao, S. He, P. Lee, J. Sun, F. Gao, L. Yang, Q. Lin, S. Rajmohan, Z. Xu, and D. Zhang, "Fighting the fog of war: Automated incident detection for cloud systems," in *2021 USENIX Annual Technical Conference (USENIX ATC 21)*. USENIX Association, Jul. 2021, pp. 131–146. [Online]. Available: https://www.usenix.org/conference/atc21/presentation/li-liqun

[60] A. Morse, "Investigation: Wannacry cyber attack and the NHS," 2017, national Audit Office UK.

[61] S. M. T. I. Tonmoy, S. M. M. Zaman, V. Jain, A. Rani, V. Rawte, A. Chadha, and A. Das, "A comprehensive survey of hallucination mitigation techniques in large language models," 2024. [Online]. Available: https://arxiv.org/abs/2401.01313

[62] DeepSeek-AI, D. Guo, D. Yang *et al.*, "DeepSeek-R1: Incentivizing reasoning capability in LLMs via reinforcement learning," 2025. [Online]. Available: https://arxiv.org/abs/2501.12948

[63] O. Ayala and P. Bechard, "Reducing hallucination in structured outputs via retrieval-augmented generation," in *Proceedings of the 2024 Conference of the North American Chapter of the Association for Computational Linguistics: Human Language Technologies (Volume 6: Industry Track)*, Y. Yang, A. Davani, A. Sil, and A. Kumar, Eds. Mexico City, Mexico: Association for Computational Linguistics, Jun. 2024, pp. 228–238. [Online]. Available: https://aclanthology.org/2024.naacl-industry.19/

[64] X. Wang, J. Wei, D. Schuurmans, Q. V. Le, E. H. Chi, S. Narang, A. Chowdhery, and D. Zhou, "Self-consistency improves chain of thought reasoning in language models," in *The Eleventh International Conference on Learning Representations, ICLR Kigali, Rwanda*, 2023.

[65] X. Chen, R. Aksitov, U. Alon, J. Ren, K. Xiao, P. Yin, S. Prakash, C. Sutton, X. Wang, and D. Zhou, "Universal self-consistency for large language model generation," 2023. [Online]. Available: https://arxiv.org/abs/2311.17311

[66] Y. Weng, M. Zhu, F. Xia, B. Li, S. He, S. Liu, B. Sun, K. Liu, and J. Zhao, "Large language models are better reasoners with self-verification," in *Findings of the Association for Computational Linguistics: EMNLP*, H. Bouamor, J. Pino, and K. Bali, Eds. Singapore: Association for Computational Linguistics, Dec. 2023, pp. 2550–2575. [Online]. Available: https://aclanthology.org/2023.findings-emnlp.167/

[67] A. Madaan, N. Tandon, P. Gupta, S. Hallinan, L. Gao, S. Wiegreffe, U. Alon, N. Dziri, S. Prabhumoye, Y. Yang, S. Gupta, B. P. Majumder, K. Hermann, S. Welleck, A. Yazdanbakhsh, and P. Clark, "Self-refine: iterative refinement with self-feedback," in *Proceedings of the 37th International Conference on Neural Information Processing Systems*, ser. NIPS '23. Red Hook, NY, USA: Curran Associates Inc., 2023.

[68] M. Roesch, "Snort - lightweight intrusion detection for networks," in *Proceedings of the 13th USENIX Conference on System Administration*, ser. LISA '99. USA: USENIX Association, 1999, p. 229–238.

[69] B. E. Strom, A. Applebaum, D. P. Miller, K. C. Nickels, A. G. Pennington, and C. B. Thomas, "Mitre ATT&CK: Design and philosophy," in *Technical report*. MITRE, 2018.

[70] Y. Wang, H. Ivison, P. Dasigi, J. Hessel, T. Khot, K. R. Chandu, D. Wadden, K. MacMillan, N. A. Smith, I. Beltagy, and H. Hajishirzi, "How far can camels go? exploring the state of instruction tuning on open resources," 2023. [Online]. Available: https://arxiv.org/abs/2306.04751

[71] H. Yu, T. Cheng, Y. Cheng, and R. Feng, "FineMedLM-o1: Enhancing the medical reasoning ability of LLM from supervised fine-tuning to test-time training," 2025. [Online]. Available: https://arxiv.org/abs/2501.09213

[72] MITRE, "CVE," 2022. [Online]. Available: https://cve.mitre.org/

[73] P. Lewis, E. Perez, A. Piktus, F. Petroni, V. Karpukhin, N. Goyal, H. Küttler, M. Lewis, W.-t. Yih, T. Rocktäschel *et al.*, "Retrieval-augmented generation for knowledge-intensive NLP tasks," *Advances in neural information processing systems*, vol. 33, pp. 9459–9474, 2020.

[74] P. E. Kaloroumakis and M. J. Smith, "Toward a knowledge graph of cybersecurity countermeasures," The MITRE Corporation, Annapolis Junction, MD, Technical Report, 2021, approved for

Public Release; Distribution Unlimited. [Online]. Available: https://d3fend.mitre.org/resources/D3FEND.pdf
[75] S. Jha, R. R. Arora, Y. Watanabe *et al.*, "ITBench: Evaluating AI agents across diverse real-world IT automation tasks," in *Proceedings of the 42nd International Conference on Machine Learning*, ser. Proceedings of Machine Learning Research, A. Singh, M. Fazel, D. Hsu, S. Lacoste-Julien, F. Berkenkamp, T. Maharaj, K. Wagstaff, and J. Zhu, Eds., vol. 267. PMLR, 13–19 Jul 2025, pp. 27 134–27 197. [Online]. Available: https://proceedings.mlr.press/v267/jha25a.html
[76] S. García, M. Grill, J. Stiborek, and A. Zunino, "An empirical comparison of botnet detection methods," *Computers & Security*, vol. 45, pp. 100–123, 2014. [Online]. Available: https://www.sciencedirect.com/science/article/pii/S0167404814000923
[77] D. Y. Huang, M. M. Aliapoulios, V. G. Li, L. Invernizzi, E. Bursztein, K. McRoberts, J. Levin, K. Levchenko, A. C. Snoeren, and D. McCoy, "Tracking ransomware end-to-end," in *2018 IEEE Symposium on Security and Privacy (SP)*, 2018, pp. 618–631.
[78] I. Sharafaldin, A. Habibi Lashkari, and A. A. Ghorbani, "Toward generating a new intrusion detection dataset and intrusion traffic characterization," in *Proceedings of the 4th International Conference on Information Systems Security and Privacy - ICISSP*, INSTICC. SciTePress, 2018, pp. 108–116, kaggle page: https://www.kaggle.com/datasets/solarmainframe/ids-intrusion-csv/data.
[79] M. Landauer, F. Skopik, and M. Wurzenberger, "Introducing a new alert data set for multi-step attack analysis," in *Proceedings of the 17th Cyber Security Experimentation and Test Workshop*, ser. CSET '24. New York, NY, USA: Association for Computing Machinery, 2024, p. 41–53. [Online]. Available: https://doi.org/10.1145/3675741.3675748
[80] Wazuh Inc, "Wazuh - the open source security platform," 2022. [Online]. Available: https://wazuh.com/
[81] K. Hammar and R. Stadler, "The CSLE-IDS-2024 dataset," Feb. 2024. [Online]. Available: https://doi.org/10.5281/zenodo.10706475
[82] AT&T Cybersecurity, "AlienVault Open Threat Exchange (OTX)," https://otx.alienvault.com, 2021.
[83] K. Hammar and R. Stadler, "Intrusion prevention through optimal stopping," *IEEE Transactions on Network and Service Management*, vol. 19, no. 3, pp. 2333–2348, 2022.
[84] K. Hammar, "Optimal security response to network intrusions in it systems," Ph.D. dissertation, KTH Royal Institute of Technology, 2024.
[85] Y. A. Yadkori, I. Kuzborskij, D. Stutz, A. György, A. Fisch, A. Doucet, I. Beloshapka, W.-H. Weng, Y.-Y. Yang, C. Szepesvári, A. T. Cemgil, and N. Tomasev, "Mitigating LLM hallucinations via conformal abstention," 2024. [Online]. Available: https://arxiv.org/abs/2405.01563
[86] D. Bertsekas, *Rollout, Policy Iteration, and Distributed Reinforcement Learning*, ser. Athena scientific optimization and computation series. Athena Scientific, 2021.
[87] ——, *Dynamic Programming and Optimal Control, Vol. II*, 3rd ed. Athena Scientific, 2007.
[88] M. Standen, M. Lucas, D. Bowman, T. J. Richer, J. Kim, and D. Marriott, "Cyborg: A gym for the development of autonomous cyber agents," *CoRR*, 2021, https://arxiv.org/abs/2108.09118.

APPENDIX A
TESTBED CONFIGURATION

The configuration of the infrastructure that we run on our testbed (as described in §IV-B) is listed in Table 5 and the network topology is shown in Fig. 17.

APPENDIX B
EXAMPLE PROMPT TEMPLATE

All of our prompt templates are available at [20]. We provide an example prompt template in the box to the right.

Prompt template for generating a response action

Below is a system description, a sequence of network logs (e.g., from an intrusion detection system), a description of a cybersecurity incident, the current state of the recovery from the incident, a list of previously executed recovery actions, and an instruction that describes a task. Write a response that appropriately completes the request. Before generating the response, think carefully about the system, the logs, and the instruction, then create a step-by-step chain of thoughts to ensure a logical and accurate response.

System:... ### Logs:... ### Incident:... ### State:...

Previous recovery actions: ...

Instruction: You are a security operator with advanced knowledge in cybersecurity and IT systems. You have been given information about a security incident and should generate the next suitable action for recovering the system from the incident. Your suggested action should be based on the logs, the system description, the current state, and the previous recovery actions only. Make sure that the suggested recovery action is consistent with the system description and the logs and that you do not repeat any action that has already been performed. The goal when selecting the recovery action is to change the state so that one of the state properties that is currently 'false' becomes 'true'. The ideal recovery action sequence is: 1. contain the attack 2. gather information 3. preserve evidence 4. eradicate the attacker 5. harden the system 6. recover operational services. When selecting the recovery action, make sure that it is concrete and actionable and minimizes unnecessary service disruptions. Vague or unnecessary actions will not change the state and should be avoided. Return a JSON object with two properties: 'Action' and 'Explanation', both of which should be strings. The property 'Action' should be a string that concisely describes the concrete recovery action. The property 'Explanation' should be a string that concisely explains why you selected the recovery action and motivates why the action is needed.
Response: <think>

APPENDIX C
PROOF OF PROPOSITION 1

We start by noting that the planning problem in §IV-D can be viewed as a stochastic shortest path problem on the graph of recovery states, where the goal is to reach the state $\mathbf{s}_t = (1, 1, 1, 1, 1, 1)$ as quickly as possible. Consequently, the problem is well-defined under standard assumptions, see e.g., [87] for details. The main approach for proving Prop. 1 is to bound the difference in estimated recovery time of a non-hallucinated action and a hallucinated action. To this end, we start by stating and proving the following lemma. (For ease of notation, we present the proof here for the case where $c(\mathbf{s}_t, \mathbf{a}_t) = 1$ for all states $\mathbf{s}_t$ and actions $\mathbf{a}_t$; the proof can be straightforwardly extended to general cost functions.)

Lemma 1. *Given the conditions of Prop. 1, we have*

$$\|\tilde{J} - J\|_\infty \leq \eta \|\tilde{J}\|_\infty \|J\|_\infty,$$

where J is the recovery time-to-go function [cf. Def. 3] and $\tilde{J}$ is the time-to-go function estimated by the LLM.

Proof. We first note that the vocabulary (i.e., the set of tokens) of any LLM is finite. Therefore, the set of feasible response actions $\mathcal{A}$ is finite. As a consequence, the state predictions $p_{\boldsymbol{\theta}'}(\mathbf{s}' \mid \mathbf{s}, \mathbf{a}, \mathbf{I})$ define a transition probability matrix between (non-terminal) recovery states. We denote this matrix by $\tilde{\mathbf{F}}$ and the corresponding matrix of the real system by $\mathbf{F}$, where $\tilde{\mathbf{F}}_{\mathbf{ss}'}$

ID(s)	*Type*	*Operating system*	*Zone*	*Services*	*Vulnerabilities*
1	Gateway	Ubuntu 20	-	Snort (ruleset v2.9.17.1), SSH, OpenFlow v1.3, Ryu SDN controller	-
2	Gateway	Ubuntu 20	DMZ	Snort (ruleset v2.9.17.1), SSH, OVS v2.16, OpenFlow v1.3	-
28	Gateway	Ubuntu 20	R&D	Snort (ruleset v2.9.17.1), SSH, OVS v2.16, OpenFlow v1.3	-
3,12	Switch	Ubuntu 22	DMZ	SSH, OpenFlow v1.3, OVS v2.16	-
21, 22	Switch	Ubuntu 22	-	SSH, OpenFlow v1.3, OVS v2.16	-
23	Switch	Ubuntu 22	Admin	SSH, OpenFlow v1.3, OVS v2.16	-
29-48	Switch	Ubuntu 22	R&D	SSH, OpenFlow v1.3, OVS v2.16	-
13-16	Honeypot	Ubuntu 20	DMZ	SSH, SNMP, PostgreSQL, NTP	-
17-20	Honeypot	Ubuntu 20	DMZ	SSH, IRC, SNMP, PostgreSQL	-
4	App node	Ubuntu 20	DMZ	HTTP, DNS, SSH	CWE-1391
5, 6	App node	Ubuntu 20	DMZ	SSH, SNMP, PostgreSQL, NTP	-
7	App node	Ubuntu 20	DMZ	HTTP, Telnet, SSH	CWE-1391
8	App node	Debian Jessie	DMZ	FTP, SSH, Apache 2, SNMP	CVE-2015-3306
9,10	App node	Ubuntu 20	DMZ	NTP, IRC, SNMP, SSH, PostgreSQL	-
11	App node	Debian Jessie	DMZ	Apache 2, SMTP, SSH	CVE-2016-10033
24	Admin system	Ubuntu 20	Admin	HTTP, DNS, SSH	CWE-1391
25	Admin system	Ubuntu 20	Admin	FTP, MongoDB, SMTP, Tomcat, Teamspeak 3, SSH	-
26	Admin system	Ubuntu 20	Admin	SSH, SNMP, Postgres, NTP	-
27	Admin system	Ubuntu 20	Admin	FTP, MongoDB, SMTP, Tomcat, Teamspeak 3, SSH	CWE-1391
49-59	Compute node	Ubuntu 20	R&D	Spark, HDFS	-
60	Compute node	Debian Wheezy	R&D	Spark, HDFS, Apache 2, SNMP, SSH	CVE-2014-6271
61	Compute node	Debian 9.2	R&D	IRC, Apache 2, SSH	CWE-89
62	Compute node	Debian Jessie	R&D	Spark, HDFS, Teamspeak 3, Tomcat, SSH	CVE-2010-0426
63	Compute node	Debian Jessie	R&D	SSH, Spark, HDFS	CVE-2015-5602
64	Compute node	Debian Jessie	R&D	Samba, NTP, SSH, Spark, HDFS	CVE-2017-7494

TABLE 5: Configuration of the IT infrastructure we run in our testbed. The network topology is shown in Fig. 17.

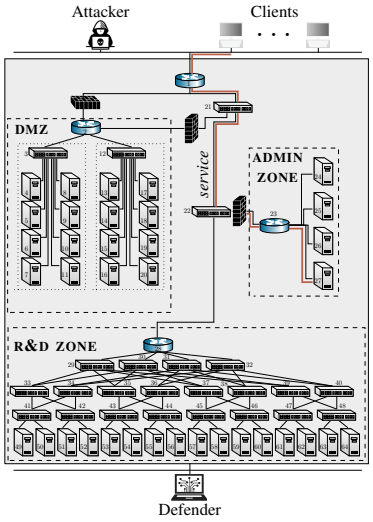

Fig. 17: The IT infrastructure that we use to collect log data for fine-tuning.

denotes the transition probability between the non-terminal states $\mathbf{s}$ and $\mathbf{s}'$. Similarly, we use $\mathbf{J}$ and $\tilde{\mathbf{J}}$ to denote the vectors obtained by applying the functions J and $\tilde{J}$ to the set of non-terminal recovery states $\tilde{\mathcal{S}}$, i.e., all states for which $\mathbf{s} \neq (1,1,1,1,1,1)$, where $\mathbf{J}_\mathbf{s}$ denotes the expected recovery time-to-go from the non-terminal state $\mathbf{s}$.

Since the goal is to minimize the recovery time, we can express the recovery time-to-go function recursively by defining a stage cost of 1 for each response action taken. Using this formulation of the recovery time-to-go, we have

$$\mathbf{J} = \mathbf{1} + \mathbf{F}\mathbf{J} \quad \text{and} \quad \tilde{\mathbf{J}} = \mathbf{1} + \tilde{\mathbf{F}}\tilde{\mathbf{J}}, \tag{6}$$

where $\mathbf{1}$ denotes the vector of all ones. Given these Bellman equations, the difference $\tilde{\mathbf{J}} - \mathbf{J}$ can be written as

$$\tilde{\mathbf{J}} - \mathbf{J} = (\mathbb{1} - \tilde{\mathbf{F}})^{-1}(\tilde{\mathbf{F}} - \mathbf{F})\mathbf{J}, \tag{7}$$

where $\mathbb{1}$ denotes the identity matrix.

Since $\|J\|_\infty$ and $\|\tilde{J}\|_\infty$ are assumed finite, $\|\mathbf{J}\|_\infty$ and $\|\tilde{\mathbf{J}}\|_\infty$ are also finite. As a consequence, the linear systems in (6) have unique solutions. Consequently, the inverse in (7) exists. Taking the supremum norm on both sides of the final expression in (7), we have

$$\begin{aligned}\|\tilde{\mathbf{J}} - \mathbf{J}\|_\infty &= \|(\mathbb{1} - \tilde{\mathbf{F}})^{-1}(\tilde{\mathbf{F}} - \mathbf{F})\mathbf{J}\|_\infty \\ &\leq \|(\mathbb{1} - \tilde{\mathbf{F}})^{-1}\|_\infty \|(\tilde{\mathbf{F}} - \mathbf{F})\mathbf{J}\|_\infty,\end{aligned} \tag{8}$$

where the last inequality follows from the sub-multiplicative property of the supremum norm. Hence, it suffices to show that the right-hand side in (8) is bounded by $\eta\|\tilde{J}\|_\infty\|J\|_\infty$. In view of (6), we have

$$\tilde{\mathbf{J}} = \mathbf{1} + \tilde{\mathbf{F}}\tilde{\mathbf{J}} \implies \|\tilde{\mathbf{J}}\|_\infty = \|(\mathbb{1} - \tilde{\mathbf{F}})^{-1}\mathbf{1}\|_\infty.$$

Since $\|\tilde{J}\|_\infty$ is assumed finite, the expected time to reach the terminal state $\mathbf{s} = (1,1,1,1,1,1)$ from any non-terminal state $\mathbf{s} \in \tilde{\mathcal{S}}$ is finite. As a consequence, the spectral radius of the transition matrix between the non-terminal states, i.e., $\tilde{\mathbf{F}}$, must be strictly less than 1. Therefore, we can expand $(\mathbb{1} - \tilde{\mathbf{F}})^{-1}$ using the Neumann series representation as $\sum_{k=0}^{\infty} \tilde{\mathbf{F}}^k$. Because the matrix $\tilde{\mathbf{F}}$ is non-negative, all of its powers are also non-negative. As a consequence, $(\mathbb{1} - \tilde{\mathbf{F}})^{-1}$ is non-negative. For any non-negative matrix $\mathbf{A}$, we have $\|\mathbf{A}\|_\infty = \|\mathbf{A}\mathbf{1}\|_\infty$. Consequently, we obtain

$$\|\tilde{\mathbf{J}}\|_\infty = \|(\mathbb{1} - \tilde{\mathbf{F}})^{-1}\mathbf{1}\|_\infty = \|(\mathbb{1} - \tilde{\mathbf{F}})^{-1}\|_\infty. \tag{9}$$

Now consider the second factor in the right-hand side of (8), i.e., $\|(\tilde{\mathbf{F}} - \mathbf{F})\mathbf{J}\|_\infty$. Fix any recovery state $\mathbf{s}$. We have

$$\begin{aligned}&\left|\left(\left(\tilde{\mathbf{F}} - \mathbf{F}\right)\mathbf{J}\right)_\mathbf{s}\right| = \left|\sum_{\mathbf{s}' \in \tilde{\mathcal{S}}} \left(\tilde{\mathbf{F}}_{\mathbf{s}\mathbf{s}'} - \mathbf{F}_{\mathbf{s}\mathbf{s}'}\right)\mathbf{J}_{\mathbf{s}'}\right| \\ &\overset{(a)}{\leq} \sum_{\mathbf{s}' \in \tilde{\mathcal{S}}} \left|\tilde{\mathbf{F}}_{\mathbf{s}\mathbf{s}'} - \mathbf{F}_{\mathbf{s}\mathbf{s}'}\right| \cdot |\mathbf{J}_{\mathbf{s}'}| \leq \left(\sum_{\mathbf{s}' \in \tilde{\mathcal{S}}} \left|\tilde{\mathbf{F}}_{\mathbf{s}\mathbf{s}'} - \mathbf{F}_{\mathbf{s}\mathbf{s}'}\right|\right) \|\mathbf{J}\|_\infty \\ &\leq \eta\|\mathbf{J}\|_\infty,\end{aligned}$$

where we use the triangle inequality to move the absolute value inside the sum and then the fact that $|ab| = |a||b|$ to obtain (a). Since this bound holds for any state $\mathbf{s}$, we have

$$\|(\tilde{\mathbf{F}} - \mathbf{F})\mathbf{J}\|_\infty \leq \eta \|\mathbf{J}\|_\infty.$$

Substituting this bound and (9) into (8) yields

$$\|\tilde{\mathbf{J}} - \mathbf{J}\|_\infty \leq \|(\mathbb{1} - \tilde{\mathbf{F}})^{-1}\|_\infty \|(\tilde{\mathbf{F}} - \mathbf{F})\mathbf{J}\|_\infty \leq \eta \|\tilde{\mathbf{J}}\|_\infty \|\mathbf{J}\|_\infty.$$

Since the recovery time-to-go from the terminal state is 0 [cf. Def. 3], we have $\|\tilde{\mathbf{J}} - \mathbf{J}\|_\infty = \|\tilde{J} - J\|_\infty$, $\|\tilde{\mathbf{J}}\|_\infty = \|\tilde{J}\|_\infty$, and $\|\mathbf{J}\|_\infty = \|J\|_\infty$. The proof is thus complete. □

Given Lemma 1, we are now ready to derive the proof of Prop. 1. The event that a hallucinated action $\hat{\mathbf{a}}$ is selected over a non-hallucinated action $\tilde{\mathbf{a}}$ in (5) implies $\tilde{Q}(\tilde{\mathbf{s}}, \hat{\mathbf{a}}) \leq \tilde{Q}(\tilde{\mathbf{s}}, \tilde{\mathbf{a}})$. To show that this inequality cannot hold under the proposition's assumptions, we start by bounding the difference between $\tilde{Q}$ and Q, where $Q(\mathbf{s}, \mathbf{a})$ is the true expected recovery time-to-go when taking response action $\mathbf{a}$ in state $\mathbf{s}$ and $\tilde{Q}(\mathbf{s}, \mathbf{a})$ is the LLM's estimate. We have

$$\begin{aligned}
&|\tilde{Q}(\mathbf{s}, \mathbf{a}) - Q(\mathbf{s}, \mathbf{a})| = \\
&\left| \sum_{\mathbf{s}' \in \tilde{\mathcal{S}}} p_{\boldsymbol{\theta}'}(\mathbf{s}' \mid \mathbf{s}, \mathbf{a}, \mathbf{I}) \tilde{J}(\mathbf{s}') - \sum_{\mathbf{s}' \in \tilde{\mathcal{S}}} P(\mathbf{s}' \mid \mathbf{s}, \mathbf{a}, \mathbf{I}) J(\mathbf{s}') \right| \\
&\quad \sum_{\mathbf{s}' \in \tilde{\mathcal{S}}} p_{\boldsymbol{\theta}'}(\mathbf{s}' \mid \mathbf{s}, \mathbf{a}, \mathbf{I}) J(\mathbf{s}') - \sum_{\mathbf{s}' \in \tilde{\mathcal{S}}} p_{\boldsymbol{\theta}'}(\mathbf{s}' \mid \mathbf{s}, \mathbf{a}, \mathbf{I}) J(\mathbf{s}') \Bigg| \\
&= \left| \sum_{\mathbf{s}' \in \tilde{\mathcal{S}}} p_{\boldsymbol{\theta}'}(\mathbf{s}' \mid \mathbf{s}, \mathbf{a}, \mathbf{I}) \left(\tilde{J}(\mathbf{s}') - J(\mathbf{s}') \right) - \right. \\
&\quad \left. \sum_{\mathbf{s}' \in \tilde{\mathcal{S}}} \left(P(\mathbf{s}' \mid \mathbf{s}, \mathbf{a}, \mathbf{I}) - p_{\boldsymbol{\theta}'}(\mathbf{s}' \mid \mathbf{s}, \mathbf{a}, \mathbf{I}) \right) J(\mathbf{s}') \right| \\
&\overset{(a)}{\leq} \sum_{\mathbf{s}' \in \tilde{\mathcal{S}}} \left| p_{\boldsymbol{\theta}'}(\mathbf{s}' \mid \mathbf{s}, \mathbf{a}, \mathbf{I}) \left(\tilde{J}(\mathbf{s}') - J(\mathbf{s}') \right) \right| + \\
&\quad \sum_{\mathbf{s}' \in \tilde{\mathcal{S}}} \left| \left(P(\mathbf{s}' \mid \mathbf{s}, \mathbf{a}, \mathbf{I}) - p_{\boldsymbol{\theta}'}(\mathbf{s}' \mid \mathbf{s}, \mathbf{a}, \mathbf{I}) \right) J(\mathbf{s}') \right| \\
&\overset{(b)}{\leq} \sum_{\mathbf{s}' \in \tilde{\mathcal{S}}} \left| p_{\boldsymbol{\theta}'}(\mathbf{s}' \mid \mathbf{s}, \mathbf{a}, \mathbf{I}) \left(\tilde{J}(\mathbf{s}') - J(\mathbf{s}') \right) \right| + \\
&\quad \sum_{\mathbf{s}' \in \tilde{\mathcal{S}}} \left| p_{\boldsymbol{\theta}'}(\mathbf{s}' \mid \mathbf{s}, \mathbf{a}, \mathbf{I}) - P(\mathbf{s}' \mid \mathbf{s}, \mathbf{a}, \mathbf{I}) \right| \|J\|_\infty \\
&\leq \|\tilde{J} - J\|_\infty + \eta \|J\|_\infty \overset{(c)}{\leq} \underbrace{\eta \|\tilde{J}\|_\infty \|J\|_\infty + \eta \|J\|_\infty}_{=\Delta},
\end{aligned}$$

where (a) follows from the triangle inequality; (b) uses the fact that $\|\mathbf{ab}\|_\infty \leq \|\mathbf{a}\|_\infty \|\mathbf{b}\|_\infty$; and (c) follows from Lemma 1. This bound implies that

$$Q(\mathbf{s}, \mathbf{a}) - \Delta \leq \tilde{Q}(\mathbf{s}, \mathbf{a}) \leq Q(\mathbf{s}, \mathbf{a}) + \Delta. \tag{10}$$

Now, if a hallucinated action $\hat{\mathbf{a}}$ is selected over a non-hallucinated action $\tilde{\mathbf{a}}$ in (5), we must have $\tilde{Q}(\mathbf{s}, \hat{\mathbf{a}}) \leq \tilde{Q}(\mathbf{s}, \tilde{\mathbf{a}})$. Combining this inequality with (10), we have

$$\begin{aligned}
&Q(\mathbf{s}, \hat{\mathbf{a}}) - \Delta \leq \tilde{Q}(\mathbf{s}, \hat{\mathbf{a}}) \leq \tilde{Q}(\mathbf{s}, \tilde{\mathbf{a}}) \leq Q(\mathbf{s}, \tilde{\mathbf{a}}) + \Delta \\
&\implies Q(\mathbf{s}, \hat{\mathbf{a}}) - Q(\mathbf{s}, \tilde{\mathbf{a}}) \leq 2\Delta.
\end{aligned} \tag{11}$$

Next, since $\hat{\mathbf{a}}$ is hallucinated and $\tilde{\mathbf{a}}$ is not, we have

$$\begin{aligned}
Q(\mathbf{s}, \hat{\mathbf{a}}) &= 1 + \mathbb{E}_{\mathbf{s}'}[J(\mathbf{s}') \mid \hat{\mathbf{a}}, \mathbf{s}, \mathbf{I}] = 1 + J(\mathbf{s}), \\
Q(\mathbf{s}, \tilde{\mathbf{a}}) &= 1 + \mathbb{E}_{\mathbf{s}'}[J(\mathbf{s}') \mid \tilde{\mathbf{a}}, \mathbf{s}, \mathbf{I}] \leq 1 + J(\mathbf{s}) - \delta.
\end{aligned}$$

Substituting $Q(\mathbf{s}, \hat{\mathbf{a}}) = 1 + J(\mathbf{s})$ into the inequality, we obtain

$$\begin{aligned}
&Q(\mathbf{s}, \hat{\mathbf{a}}) \geq Q(\mathbf{s}, \tilde{\mathbf{a}}) + \delta \implies \delta \leq Q(\mathbf{s}, \hat{\mathbf{a}}) - Q(\mathbf{s}, \tilde{\mathbf{a}}) \leq 2\Delta \\
&= 2 \left(\eta \|\tilde{J}\|_\infty \|J\|_\infty + \eta \|J\|_\infty \right) = 2\eta \|J\|_\infty \left(\|\tilde{J}\|_\infty + 1 \right).
\end{aligned}$$

Since the conditions of the proposition state that

$$\delta > 2\eta \|J\|_\infty \left(\|\tilde{J}\|_\infty + 1 \right),$$

we conclude that whenever a non-hallucinated action exists, it will be selected by the minimization (5). □

APPENDIX D
NOTATION

Our notation is summarized in Table 6.

Notation(s)	*Description*
$\mathbf{a}$, T	Response action; cf. §IV-D, recovery time; cf. §IV-D.
$\mathbf{s}$, $\tilde{\mathbf{s}}$	Recovery state [cf. (3)] and predicted state.
$\mathbf{I}$	Initial information about the incident (e.g., logs).
$p_{\boldsymbol{\theta}}$, $\boldsymbol{\theta}$	the token distribution of an LLM and its parameters; cf. (1).
$\boldsymbol{\theta}'$	Fine-tuned parameter vector of an LLM; cf. §IV-B.
$\mathcal{D}$	Instruction dataset for fine-tuning; cf. §IV-B.
$\mathbf{x}, \mathbf{y}$	Instruction and desired output; cf. §IV-B.
N	Number of candidate actions to evaluate; cf. §IV-D.
M	Number of samples to estimate expected values in Alg. 1.
$\hat{\mathbf{a}}_t$	The response action selected after planning; cf. (5).
$J, \tilde{J}$	Recovery time-to-go functions (true and estimated); cf.§IV-D.
$Q, \tilde{Q}$	Q-functions (true and estimated by LLM); cf. §IV-D.
$\mathcal{S}, \mathcal{A}$	Sets of recovery states and response actions; cf. §IV-D.
$\tilde{\mathcal{S}}$	Set of non-terminal recovery states; cf. §IV-D.
$\mathcal{A}_t^N$	The set of N candidate actions at time step t; cf. §IV-D.

TABLE 6: Notation.

APPENDIX E
EXPERIMENTAL SETUP

All computations are performed using 4×QUADRO RTX 8000 GPUS. The hyperparameters that we use for fine-tuning and for instantiating PPO are listed in Table 7. Parameters not listed in Table 7 are set to default values.

Parameter(s)	*Value(s)*
LORA rank r,α, dropout,learning rate	64, 128, 0.05, 0.00095
Batch size, gradient accumulation steps	5, 16
Temperature, training epochs,quantization	0.6, 2, 4 bit
PPO [19, Alg. 1]	
Learning rate, # hidden layers	$5148 \cdot 10^{-5}$, 1,
# Neurons/layer,# steps/update	64, 2048
Batch size, discount factor γ	16, 0.99
GAE λ, clip range, entropy coefficient	0.95, 0.2, $2 \cdot 10^{-4}$
Value coefficient, max gradient norm	0.102, 0.5
Feature representation	cyborg features [88] & one-hot encoded scan/decoy states

TABLE 7: Hyperparameters.

APPENDIX F
ARTIFACT APPENDIX

All results presented in this paper are fully reproducible using open-source software and data. To enable independent verification of our results and encourage future research, we release a complete set of artifacts that allow the community to build upon our work without additional engineering effort. Specifically, we release the following artifacts:

- A dataset of $68,000$ incidents and response plans, which can be used for fine-tuning LLMs for incident response. The dataset is generated based on a combination of real attacks executed on our testbed and synthetic data.
- The weights of the fine-tuned LLM that we use to produce the results reported in the paper. This LLM has 14 billion parameters and is derived from the DEEPSEEK-R1 LLM.
- Python code for downloading the fine-tuning dataset.
- Python code for downloading the fine-tuned LLM.
- Python code for generating a response action.
- Python code for fine-tuning the LLM.
- A video demonstration of our incident response system.

The following subsections describe how to access the artifacts and the setup required to use them.

A. Artifact Dependencies

All artifacts are publicly available at https://doi.org/10.5281/zenodo.17770990. The code can be accessed at https://github.com/Kim-Hammar/llm_incident_response_ndss26 and is released under the CC-BY-SA 4.0 license.

Hardware dependencies. The hardware requirements for our software artifacts (i.e., the Python scripts) are listed in Table 8 on the next page. The non-software artifacts (i.e., the dataset and the weights) can be accessed at https://doi.org/10.5281/zenodo.17770990 and do not require specific hardware.

Software dependencies. The only software requirement for our artifacts is the Python library called `llm_recovery`, which is written by us and available on PYPI.[2] We have tested our artifacts on the following software platforms:

- A MacBook Pro with macOS Sequoia 15.6.1 and Python 3.11.
- A Google Cloud virtual machine with Ubuntu 22.04 and Python 3.10.
- A Google Colab notebook with Ubuntu 20.04 and Python 3.9.

Data and model dependencies. Our artifacts are self-contained. The Python scripts rely only on the dataset and model that we supply as part of our artifacts.

B. Artifact Installation & Configuration

To install our artifacts, run the following commands:

```
git clone https://github.com/Kim-Hammar/
llm_incident_response_ndss26
pip install llm_recovery==0.0.13
```

[2] https://pypi.org/project/llm-recovery/.

C. Experiment Workflow

To evaluate our software artifacts (i.e., the Python scripts), open the directory `llm_incident_response_ndss26` and follow these steps:

- (S1) `python load_fine_tuned_llm.py`
  - This step downloads the weights of our fine-tuned LLM from HUGGINGFACE.
- (S2) `python load_training_dataset.py`
  - This step downloads the dataset that we use for fine-tuning from HUGGINGFACE.
- (S3) `python response_generation.py`
  - This step samples a random incident from the fine-tuning dataset and uses the fine-tuned LLM to generate the first response action.
- (S4) `python fine_tune_llm.py`
  - This step fine-tunes the DEEPSEEK-R1-DISTILL-QWEN-14B LLM on our dataset. To reduce the execution time, we have configured the script to use a small subset of the fine-tuning dataset.

Remark 4. *Some of the Python scripts require a* GPU *to complete within a reasonable time; see Table 8. A single commodity* GPU *is sufficient, e.g.,* RTX 8000. *If no* GPU *is available, the functionality of the response-generation process can be verified through our video demonstration at https://www.youtube.com/watch?v=SCxq2ye-R4Y. The video demonstrates the decision-support system for incident response that we have developed based on the above scripts. The complete software of our system is available at https://github.com/Kim-Hammar/csle and https://github.com/Kim-Hammar/llm_recovery. This software is released for the community to build on, but is not included as an artifact in this paper.*

D. Major Claims

The main claims of our paper are as follows.

- (C1): We release the first fine-tuning dataset for incident response.
- (C2): We release the first open-source fine-tuned LLM for incident response.
- (C3): Our LLM is lightweight.
- (C4): Our method has reduced hallucination.
  - We prove this claim in Propositions 1 and 2 in the paper.
- (C5): Our method generates effective incident response plans.

E. Evaluation

This section includes the operational steps and experiments to evaluate the functionality of our artifacts and validate the major claims of our paper.

Experiment (E1).

[Access the fine-tuned LLM, the video demonstration, and the training dataset] [10 human-minutes + 0 compute-minutes]: This experiment validates claims (C1) and (C2).

Artifact	*Hardware requirements*
Load fine-tuning dataset	Commodity CPU, 8 GB RAM, 20 GB storage.
Load fine-tuned LLM	Commodity CPU, 72 GB RAM, 100 GB storage.
Generate response action	RTX 8000 GPU (or a more powerful GPU), 72 GB RAM, 100 GB storage.
Fine-tune LLM	4×RTX 8000 GPU (or a more powerful GPU), 72 GB RAM, 200 GB storage.
Video demonstration	None, access at https://www.youtube.com/watch?v=SCxq2ye-R4Y&.
Dataset for fine-tuning	None, access at https://doi.org/10.5281/zenodo.17770990.
Weights of the fine-tuned model	None, access at https://doi.org/10.5281/zenodo.17770990.

TABLE 8: The hardware requirements for our artifacts.

[How to] Access the artifacts at https://doi.org/10.5281/zenodo.17770990. The video demonstration is also available on YouTube: https://www.youtube.com/watch?v=SCxq2ye-R4Y. The setup for the demonstration is illustrated in Fig. 18.

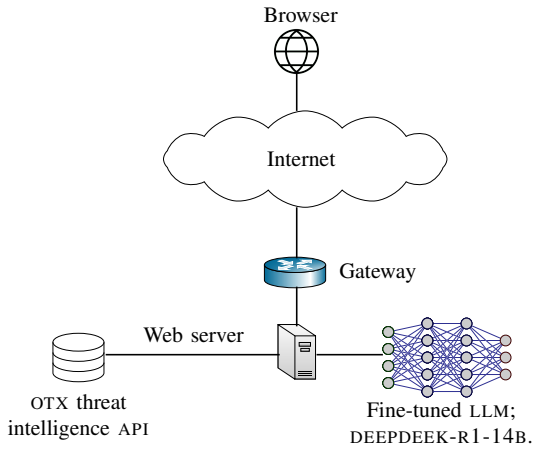

Fig. 18: Setup for the video demonstration. The fine-tuned LLM and a Python-based web server run on a SUPERMICRO 7049 server with Ubuntu 22.04, 768 GB RAM, a 24-core Intel Xeon CPU, and 4× RTX 8000 GPUs. The server hosts a web application that provides a browser-accessible user interface for our incident response decision-support system.

[Preparation] None.

[Execution] None.

[Results] Access to a dataset of 68,000 incidents and responses, the weights of a fine-tuned LLM for incident response, and a video demonstration of our incident response system.

Experiment (E2). [Download the fine-tuned LLM and the training dataset] [5 human-minutes + 5 compute-minutes]: This experiment validates claim (C3).

[How to] Complete steps (S1) and (S2) in §F-C. (If the hardware requirements for (S1) are not met, watch the video instead.)

[Preparation] Install our artifacts, as described in §F-B.

[Execution] Run the commands listed for steps (S1) and (S2) in §F-C.

[Results] The expected output of (S1) is:

```
python load_fine_tuned_llm.py
Loading the fine-tuned incident response LLM. LLM
loaded successfully.
```

The expected output of (S2) is:

```
python load_training_dataset.py
Loading training dataset.
Training dataset loaded successfully.
```

Experiment (E3). [Use the fine-tuned LLM] [5 human-minutes + 5 compute-minutes]: This experiment validates claims (C3) and (C5).

[How to] Complete step (S3) in §F-C. (If you do not have access to a GPU, watch the video demonstration instead.)

[Preparation] Install our artifacts, as described in §F-B.

[Execution] Follow step (S3) in §F-C.

[Results] The output of (S3) should be similar to:

```
python response_generation.py
I recognize that while the attack is contained,
I do not yet have enough information to fully
eradicate it. Therefore, I choose to acquire
disk and memory images along with relevant logs,
preserving evidence in a forensically sound
manner to support analysis.</think>
{
"Action": "Acquire full disk and memory images of
10.20.11.42 and export DNS, firewall, and NetFlow
logs to write-protected storage.",
"Explanation": "Capturing images and logs
secures evidence for later analysis and legal
requirements."}
```

Experiment (E4). [Fine-tune a new LLM] [5 human-minutes + 5 compute-minutes]: This experiment demonstrates the fine-tuning process. We have scaled down the experiment so that it can be completed quickly. Full fine-tuning can take several days, depending on the hardware setup.

[How to] Complete step (S4) in §F-C. (If you do not have access to a GPU, watch the video demonstration instead.)

[Preparation] Install our artifacts, as described in §F-B.

[Execution] Follow step (S4) in §F-C.

[Results] The output of (S4) should be similar to:

```
python fine_tune_llm.py
Step: 1, Epoch: 0.5000, ...
Step: 2, Epoch: 1.0000, ...
```

Acknowledgments. We thank the artifact evaluators for thoroughly verifying our code and providing valuable feedback, which helped us improve the usability of our artifacts.